Homeodomain protein 1 is an essential regulator of gene expression during sexual differentiation of malaria parasites

Riward Campelo Morillo [1], Xinran Tong [1], Wei Xie [2], Todd Lenz [3], Gayani Batugedara [3], Nusrat Tabassum [1], Lindsey M. Orchard [4], Wassim Daher [5], Dinshaw J. Patel [2], William S. Noble [6], Manuel Llinás [4,7], Karine G. Le Roch [3], Björn F.C. Kafsack [1, *]

[1] Department of Microbiology & Immunology, Weill Cornell Medicine, New York, NY 10065, USA
[2] Structural Biology Program, Memorial Sloan-Kettering Cancer Center, New York, NY 10065, USA
[3] Department of Molecular, Cell and Systems Biology, University of California Riverside, Riverside, CA 92521, USA
[4] Department of Biochemistry & Molecular Biology and Huck Center for Malaria Research, Pennsylvania State University, University Park, PA, 16802
[5] Dynamique des Interactions Membranaires Normales et Pathologiques, UMR5235 CNRS, INSERM, Université de Montpellier, Montpellier
[6] Department of Genome Sciences, University of Washington, Seattle, WA, USA
[7] Department of Chemistry, Pennsylvania State University, University Park, PA, 16802, USA.
* Corresponding Author: bkafsack@med.cornell.edu

ABSTRACT

Transmission of *Plasmodium falciparum* and other malaria parasites requires differentiation from asexual blood stages into male and female gametocytes, a non-replicative sexual stage necessary for transmission to the mosquito vector. This particular transition relies on chromatin reorganization mechanisms that coordinate the silencing and activation of a large number of stage specific genes. However, the transcriptional and chromatin regulators that mediate the changes during sexual differentiation remain largely unknown. Here, we identify the previously uncharacterized Homeodomain Protein 1 (HDP1) as an essential regulator of this process. HDP1 binds DNA in a sequence-specific manner and is tightly associated with chromatin in early gametocytes and required for the critical expansion of the inner membrane complex. Loss of HDP1 leads to deregulation of heterochromatin-associated gene silencing, decreased telomere clustering and increased chromatin accessibility. We propose that HDP1 plays a crucial role in restructuring the parasite's chromatin landscape during early sexual differentiation.

INTRODUCTION

In order to complete its life cycle, *Plasmodium falciparum*, the most widespread and virulent of the protozoan parasites that cause malaria in humans, must differentiate repeatedly into unique cell-types able access and exploit specialized niches within their human and mosquito hosts. One of these key developmental transitions occurs during the parasite's blood stage. To maintain a persistent infection within the human host, malaria parasites undergo continuous rounds of asexual replication within erythrocytes. However, these replicating asexual cells are not infectious to their mosquito vector and therefore cannot mediate transmission to the next human host. Transmission requires the formation of non-replicating male and female sexual forms, called gametocytes, that mate in the mosquito midgut after being taken up during a blood meal and develop into the motile ookinete stage that infects the mosquito. While most malaria parasite species form round gametocytes within 2-6 days, sexual differentiation in *P. falciparum* takes substantially longer, 12-14 days, and produces gametocytes with a characteristic falciform morphology that give the parasite its name.

All differentiation requires the repression and activation of genes that underlie the specific phenotypes of the origin and destination cell-types, respectively. To ensure commitment to one cell-type or another, these transitions are often controlled by a bistable switch that controls the activity of a key regulator at the top of the transcriptional cascade that underlies the differentiation program (Bhattacharya et al., 2010; Norman et al., 2015; Park et al., 2012; Satory et al., 2011). The broader downstream changes in gene expression are then accomplished by both changing the availability of specific transcription factors and changing their access to cell-type-specific promoters via chromatin re-organization.

Recent work has found that this paradigm also applies in malaria parasites, where the initiation of sexual differentiation is controlled by bistable expression of a master regulator, the transcription factor AP2-G (Kafsack et al., 2014; Sinha et al., 2014). During asexual replication the *ap2-g* locus is silenced by heterochromatin (Brancucci et al., 2014; Kafsack et al., 2014; Lopez-Rubio et al., 2009) but, due to the presence of AP2-G binding sites within its own promoter region, incomplete repression of *ap2-g* in individual cells can activate a transcriptional feedback loop that drives AP2-G expression to high levels

thereby committing cells to the gene expression program underlying sexual differentiation (Josling et al., 2020; Kafsack et al., 2014; Poran et al., 2017). Under conditions that impair heterochromatin maintenance, this feedback loop is activated in a larger fraction of cells thereby increasing the frequency of sexual differentiation (Brancucci et al., 2014; Coleman et al., 2014; Filarsky et al., 2018).

Commitment to sexual differentiation program also triggers a substantial re-distribution of heterochromatin during the early stages gametocyte development (Bunnik et al., 2018; Fraschka et al., 2018). These changes involve substantial expansion of sub-telomeric heterochromatin domains on several chromosomes to silence asexual blood-stage specific genes. One such example is a cluster of genes on chromosome 2 that are required for trafficking of PfEMP1, a parasite-encoded adhesin on the erythrocyte surface that is critical for immune evasion in asexually-replicating parasites but not expressed in gametocytes (Tibúrcio et al., 2013). Conversely, heterochromatin is lost from several loci that were previously silenced in asexual stages but upregulated during early gametocyte development (Bunnik et al., 2018; Fraschka et al., 2018).

While AP2-G is critical for the initiation of sexual differentiation, it is expressed only during a small window beginning with sexually committed schizonts and is no longer required after the first 48 hours of gametocyte development (Bancells et al., 2019; Josling et al., 2020). This suggests that the changes in gene expression underlying gametocyte development are carried out by a second wave of transcriptional regulators, which is consistent with the observation that AP2-G upregulates a number of putative transcription factors and chromatin remodeling enzymes (Josling et al., 2020; Poran et al., 2017).

Unsurprisingly, gametocyte maturation over nearly two weeks and five distinct morphological stages is accompanied by a wide array of gene expression changes (Kent et al., 2018; Painter et al., 2017; van Biljon et al., 2019; Young et al., 2005). However, relatively little is known about the transcriptional regulators downstream of AP2-G that mediate these changes. Compared to other single-celled eukaryotes, the genomes of malaria parasites contain a small fraction of DNA binding proteins. Like AP2-G, most belong to the ApiAP2 family (Balaji et al., 2005) but only a small number have been shown to function specifically during gametocyte development (Modrzynska et al., 2017). In the

92 rodent malaria parasite *P. berghei* the DNA-binding protein PbAP2-G2 functions as a
93 transcriptional repressor of asexual-specific gene expression (Sinha et al., 2014; Yuda et
94 al., 2015), while PbAP2-FG (PyAP2-G3 in *P. yoelii*) was shown to mediate upregulation
95 of female-specific transcripts (Yuda et al., 2019; Zhang et al., 2017). Whether these
96 functions are conserved in *P. falciparum* remains to be determined.

97 In this study, we identify HDP1, a previously uncharacterized DNA-binding protein that is
98 upregulated during sexual differentiation. Parasites lacking HDP1 and are unable to
99 upregulate genes required for the expansion of the inner membrane complex and fail to
100 progress beyond the earliest stages of gametocyte development. Additionally, loss of
101 HDP1 expression results in an increase in chromatin accessibility, reduced telomere
102 clustering, and leaky transcription of heterochromatin-associated genes in early
103 gametocytes. Our findings indicate that HDP1 is an essential regulator of gene expression
104 and chromatin during early gametocytogenesis.

105 **RESULTS**

106 ***hdp1* is essential for gametocyte development.**

107 In search for possible regulators of gene expression during *P. falciparum* sexual
108 differentiation, we identified Homeodomain-like protein 1 *(hdp1, PF3D7_1466200)*
109 encoding a 3078 amino acid protein with a C-terminal homeodomain-like domain, a helix-
110 turn-helix structural motif commonly involved in DNA-binding (Figure 1A) (Bürglin and
111 Affolter, 2016). Syntenic orthologs of *hdp1* could readily be identified in other malaria
112 parasites with homology to the homeodomain-like domain extending to the coccidia but
113 apparently absent from other apicomplexan clades (Figure 1B). Analysis of *hdp1*
114 expression in *P. falciparum* blood stages by qRT-PCR detected only minimal expression
115 in asexual blood stages with substantial upregulation during the early stages of
116 gametocytogenesis (Figure 1C). AP2-G, the transcriptional master switch that initiate the
117 sexual differentiation gene expression program (Kafsack et al., 2014), binds at two sites
118 located upstream of *hdp1* coding sequence early during the gametocytogenesis (Josling
119 et al., 2020), consistent with our hypothesis that AP2-G activates additional regulators of
120 gene expression during early gametocytogenesis.

121 In an effort to determine HDP1's subcellular localization, we inserted an in-frame N-
122 terminal HaloTag at the endogenous locus (Figure S1A) in order to avoid possible
123 interference with the putative DNA-binding activity of the C-terminal homeodomain-like
124 domain. As expected, no Halo-tagged protein could be detected in asexual stages (data
125 not shown). However, when we attempted to determine Halo-HDP1 levels, we found that
126 *halo-hdp1* cultures were unable to produce the characteristic crescent shapes of maturing
127 *P. falciparum* gametocytes (Figure 2A-B). Tagging the HDP1 C-terminus with either GFP
128 or a triple Ty1 epitope tag (*hdp1-gfp* and *hdp1-Ty1*, Figure S1B-C), yielded parasite lines
129 that produce gametocytes indistinguishable in numbers and morphology from the wildtype
130 parent (Figure 2A-B), despite the proximity to the putative DNA-binding domain.

131 To test whether insertion of the N-terminal tagging resulted in a loss of HDP1 function,
132 we generated a HDP1 knockout line for comparison. We used genome editing to replace
133 1.4 kb at the 5' end of *hdp1* locus with a selectable marker cassette (Figure S1D). The
134 resulting Δ*hdp1* parasites exhibited no discernible change in phenotype in asexual blood-
135 stages, but like the *halo-hdp1* parasites, were unable to generate falciform gametocytes
136 (Figure 2D-E). More detailed analyses using synchronous induction of
137 gametocytogenesis found both *halo-hdp1* and Δ*hdp1* have sexual commitment rates
138 comparable to the NF54 parent (Figure S2A) but are unable to complete gametocyte
139 development. We found that on day 2 of development Δ*hdp1* Stage I gametocytes had
140 normal levels of viability (Figure S2B) as indicated by robust mitochondrial membrane
141 potential but had lost the ability to maintain this potential by day 5 of development when
142 gametocytes from other lines had matured to stage III (Figure 2C, F).

143 As the substantial length of the *hdp1* coding sequence made genetic complementation
144 infeasible, we generated an inducible *hdp1* knockdown parasite line by inserting a triple
145 Ty1 epitope tag followed by with the autocatalytic glmS ribozyme at the 3' end of the
146 endogenous *hdp1* coding sequence through genome editing (Figure S1E) (Prommana et
147 al., 2013). In the absence of glucosamine, the resulting *hdp1-glmS* gametocytes
148 expressed HDP1 protein at levels comparable to the *hdp1-Ty1* parasites without the
149 ribozyme and produced normal gametocytes in term of number and morphology (Figure
150 S3). Supplementation of the culture medium with 5mM glucosamine during the first 5 days

151 of gametocyte development had no discernible effect on *hdp1-Ty1* parasites but
152 diminished HDP1 expression by 70% and reduced falciform gametocytes by 80% in *hdp1-*
153 *glmS* parasites, recapitulating the phenotype of the *halo-hdp1* and Δ*hdp1* lines (Figure
154 2G-H). Since *hdp1* transcript levels remain relatively constant during gametocyte
155 development (Figure 1C), we wanted to test whether continuous expression of HDP1 was
156 required for gametocyte maturation. Knockdown of *hdp1* levels with glucosamine reduced
157 gametocyte maturation when added prior to day 5 but not thereafter, indicating that
158 sufficient HDP1 protein had been produced by that time to support gametocyte maturation
159 (Figure S3).

160 **HDP1 localizes to the nucleus of early gametocytes.**

161 An earlier study had reported a variety of subcellular localizations for HDP1, including
162 export to the erythrocyte membrane of early gametocytes, based on antibodies raised
163 against the low-complexity repeat region (Nixon et al., 2018). This was surprising given
164 the absence a predicted signal peptide or transmembrane domains and localization of the
165 *Toxoplasma gondii* ortholog to the nucleus of tachyzoites (Figure S4). To resolve this
166 apparent disagreement, we carried out live-cell and immunofluorescence microscopy in
167 gametocytes of *hdp1-gfp* and *hdp1-Ty1*, respectively. In each case, HDP1 clearly
168 localized to the gametocyte nucleus (Figure 3A-B). Analysis of HDP1 protein levels by
169 western blotting of *hdp1-Ty1* lysates with antibodies against Ty1 epitope tag detected no
170 expression in asexual blood stages but showed increasing HDP1 levels from day 2 of
171 gametocytogenesis (Stage I-II) onward, reaching maximal levels by day 5 (Stage III)
172 before dropping again by day 8 (Stage IV) (Figure 3C). Analysis of subcellular fractions
173 from day 5 *hdp1-Ty1* gametocytes showed HDP1 almost exclusively in the parasite
174 nucleus, where about 70% is resistant to solubilization with up to 600mM NaCl, indicating
175 a tight association with chromatin (Figure 3D) and validating HDP1 as a nuclear protein.

176 **The HDP1 homeodomain-like domain dimerizes to efficiently bind DNA *in vitro.***

177 To evaluate HDP1 ability to bind DNA, we expressed a GST-fusion of the HDP1 homeo-
178 domain in *E. coli.* Following protein isolation, we found that much of the fusion protein
179 remained bound to bacterial DNA but could be released by the addition of the poly-cation
180 polyethylenimine during isolation (*data not shown*). Analysis of the domain's sequence

181 specificity by protein-binding microarray showed a preference for the palindromic
182 hexamer GTGCAC (Figure 4A, Figure S5). Since homeo-domains generally recognized
183 DNA as dimers (Bürglin and Affolter, 2016; Pradhan et al., 2012), we carried out
184 isothermal titration calorimetry to measure the interaction of HDP1 with double-stranded
185 DNA containing a tandem motif with a 5 bp spacer that places the motifs one helical turn
186 apart. The results indicated optimal binding at 2:1 protein to DNA molar ratio with a
187 dissociation constant of 2.8 μM supporting DNA recognition as a dimer (Figure 4B). Next,
188 we performed DNA gel-shift assays with double-stranded probes containing either no
189 match, a single binding-motif, or a tandem motif. When compared to the tandem-motif
190 probe, the gel-shift of the single motif probe was substantially weaker but identical in size
191 (Figure 4C), again consistent with DNA recognition as a dimer. Intriguingly, a scan of the
192 3D7 reference genome for instances of GTGCAC tandem motifs with a 5-6 bp spacer
193 found them exclusively located at each chromosome end with the first tandem located
194 within either 7 or 28bp of the ultimate *rep20* sub-telomeric repeat, with the exception of
195 those ends where this region was deleted as the result of telomere healing events
196 (Calhoun et al., 2017) (Figure 4D, Data Set 1). Earlier work had predicted these
197 conserved sequences to be recognized by the ApiAP2-domain protein SIP2 in asexual
198 blood stages based on its ability to bind them *in vitro* (Flueck et al., 2010, Campbell et al.,
199 2010), however their unique spacing and palindromic nature clearly distinguishes these
200 tandem motifs from the arrays of SIP2 binding sites just downstream. While the function
201 of these motifs in asexual and sexual blood stages remains unclear, their exclusive
202 localization at chromosome ends is highly conserved across *P. falciparum* isolates (*data*
203 *not shown*).

204 **Loss of HDP1 leads to dysregulation of gene expression during early gametocyte**
205 **development.**

206 Based on HDP1's ability to bind DNA, we wanted to test whether it plays a role in the
207 regulation of gene expression during early gametocytogenesis. To minimize the change
208 of looking at the consequences of aberrant gametocyte development we decided to
209 sequence total RNA from Δ*hdp1* and parental NF54 Stage I gametocytes on Day 2 of
210 development when HDP1 is first expressed but prior to any change in viability or
211 morphology in HDP1 deficient parasites (Figure 2D, Figure S2B).

212 Global comparison of transcript abundances by RNA-seq showed that the majority of
213 genes were expressed at similar levels including the markers of very early gametocytes
214 *pfs16* and *gexp5* (Figure 5A), supporting our earlier observation that HDP1-deficient
215 parasite initiate gametocyte development at similar rates. However, we observed reduced
216 transcript levels for 188 genes and increased levels for 150 genes in Δ*hdp1* Stage I
217 gametocytes compared to those of the NF54 parent line. Gene set enrichment analysis
218 (GSEA) found that transcripts encoding components of the inner membrane complex
219 were significantly down-regulated (Figure 5B) while transcripts from heterochromatin-
220 associated multi-copy gene families were significantly over-represented among up-
221 regulated genes (Figure 5C), including members of the *var*, *rifin*, *stevor*, and *PHISTa/b/c*
222 gene families (Figure 5D, Fig S6A-B). While fold-changes for these genes could be
223 substantial, the absolute increase in transcripts for these genes was often relatively small
224 but significantly above levels in WT cells (Data Set 2), possibly indicating impaired
225 heterochromatin-mediated silencing allowing for leaky background transcription rather
226 than full transcriptional activation. Comparison of transcript levels of *var* & *rifin* family
227 genes found similar levels of upregulation regardless of whether these were located in
228 subtelomeric or non-subtelomeric regions of heterochromatin (Figure S6C). Analysis of
229 *var* gene expression in asexual Δ*hdp1* ring-stages found expression of a single major *var*
230 gene as expected for a recently cloned parasite line and indicating that mutually exclusive
231 *var* gene expression remained unaffected (Figure S6D).

232 **Loss of HDP1 increases chromatin accessibility and decreases telomeric**
233 **clustering in early gametocytes.**

234 Despite numerous attempts with the GFP- and Ty1-tagged lines, we were unable to
235 determine genome-wide binding of HDP1 by chromatin immunoprecipitation sequencing.
236 Instead, we used high-throughput chromatin-conformation capture (Hi-C) to look for
237 differences in chromatin organization of day 2 gametocytes between the NF54 and Δ*hdp1*
238 lines. While correlation analysis of Hi-C replicates indicated a clear difference between
239 these lines (Figure 6A), overall intra-chromosomal interactions appeared largely
240 unchanged (Figure S7). However, further statistical analysis revealed a genome-wide
241 reduction in long distance interactions in Δ*hdp1* (Figure 6B). Genome-wide mapping of

242 interaction changes revealed a substantial reduction in interaction frequency between
243 virtually all chromosome ends (Figure 6C), consistent with reduced but not abrogated
244 telomere clustering. Based on the small but significant upregulation of heterochromatin
245 associated genes and a reduction in telomeric clustering, we hypothesized that chromatin
246 compaction might be impaired in HDP1-deficient parasites resulting in increased
247 chromatin accessibility. Indeed, brief treatment with micrococcal nuclease (MNase)
248 revealed accelerated digestion of chromatin from Δ*hdp1* gametocytes (Figure 6D),
249 consistent with an increase in chromatin accessibility.

250 **HDP1 is required for extension of the inner membrane complex in early**
251 **gametocytes.**

252 Among the genes with reduced transcript levels in HDP1 knockout parasites, those
253 associated with the inner membrane complex were substantially enriched (Figure 5A-B,
254 Figure 7A). This was notable since Δ*hdp1* gametocytes fail to elongate from spherical
255 stage I gametocytes into the oblong Stage II, a process that depends on the extension of
256 the inner membrane complex. Six separate inner membrane complex genes were
257 confirmed by qRT-PCR to have greater than 2-fold lower transcript levels in HDP1
258 knockout gametocytes (Figure 7B). These included PhIL1 and the PhIL1-interacting
259 protein 1 (PIP1), both of which are highly upregulated in early *P. falciparum* gametocytes
260 and essential for inner membrane complex assembly and gametocyte maturation (Parkyn
261 Schneider et al., 2017). Strikingly, the spherical morphology of *hdp1*-deficient
262 gametocytes perfectly resembles the phenotype of gametocytes when PhIL1 is knocked
263 down. Comparison of PhIL1 protein levels showed a 75% percent reduction in Δ*hdp1*
264 gametocytes compared to wild-type parent (Figure 7C). The concomitant reduction in
265 PhIL1 expression (Figure 7D) and inner membrane complex extension (Figure 7E) when
266 HDP1 is knocked down with glucosamine in *hdp1-glmS* gametocytes confirmed the
267 dependence of PhIL1 expression on HDP1.

268 **DISCUSSION**

269 Our understanding of the regulatory mechanisms that control sexual differentiation in *P.*
270 *falciparum* has improved substantially in recent years. Much of this work has focused on
271 the regulation of AP2-G, the master regulator of this developmental decision. However, it

272 is becoming clear that the function of AP2-G is constrained to the initiation of the
273 transcriptional program that underlies the nearly two week-long process of forming
274 gametocytes (Bancells et al., 2019). This suggest that a second wave of hitherto unknown
275 transcriptional regulators is required drive gametocyte-specific gene expression during
276 early gametocyte development.

277 In this study, we demonstrate that HDP1 functions as an essential regulator during sexual
278 differentiation. A nuclear DNA-binding protein, HDP1 is specifically up-regulated during
279 early gametocyte development and essential for their maturation. In particular, HDP1
280 regulates the expression of genes required for the expansion of the inner membrane
281 complex that gives *P. falciparum* gametocytes their characteristic crescent shape. While
282 HDP1 expression in *P. falciparum* is gametocyte specific, its *P. berghei* ortholog
283 (PBANKA_1329600) may also function during asexual blood-stage replication as its
284 disruption leads to significant reduction in growth. This suggests that the gametocyte-
285 specific function of HDP1 may have evolved more recently in the Laveranian clade of
286 malaria parasites which produce crescent gametocytes. While absent from the asexual
287 blood-stages and essential during early gametocyte development, whether HDP1 is
288 required in other parasite stages remains to be determined. Since the knockdown system
289 used in this study regulates expression at the transcript level, we can infer that additional
290 translation of HDP1 is not required during the later stages of gametocyte maturation but
291 HDP1 protein expressed during the earlier stages may well be required throughout
292 gametocyte development. Previous transcriptomic studies indicate that HDP1 is also
293 expressed in ookinetes, suggesting a role even following mating. Intriguingly,
294 homeodomain-like proteins have been implicated in mating processes of other haploid
295 protozoa, such as Dictyostelium (Hedgethorne et al., 2017).

296 We also found that HDP1 is required for efficient heterochromatin-mediated gene
297 silencing during sexual differentiation. In gametocytes lacking HDP1, we observed low
298 but significant up-regulation across a wide array of heterochromatin-associated gene
299 families. Chromosome conformation capture analysis showed broad alterations to
300 chromatin organization in HDP1-deficient parasites with an overall reduction in long-
301 distance interactions that was most pronounced at the end of chromosomes, consistent

302 with reduced, but not ablated, clustering of the sub-telomeric heterochromatin regions in
303 the nuclear periphery. While its cognate DNA motifs are exclusively found at the boundary
304 of the subtelomeric repeats, localization of HDP1 appeared evenly distributed throughout
305 the gametocyte nucleus rather than in foci at the nuclear periphery, suggesting that the
306 HDP1 does not localize to these sites exclusively. One explanation is that HDP1 promotes
307 chromatin packaging, leading to an overall increase in chromatin accessibility observed
308 in HDP1 deficient cells. This would also explain the leaky expression of heterochromatin-
309 associated genes as efficient silencing depends on limiting promoter accessibility while
310 the promoters of euchromatin-associated genes are already generally accessible and a
311 reduction in packaging would therefore be predicted to have little impact on transcript
312 levels.

313 Additional studies will focus on identifying interaction partners of HDP1 and elucidating
314 its the structure-function relationship. Only 2% of its protein sequence is comprised of the
315 homeodomain-like DNA-binding domain while the remainder contains no other
316 identifiable domains and conservation is generally weak outside this region. The fact that
317 insertion of a large tag at the N-terminus results in loss of function indicates that critical
318 interactions occur in this region but which other regions are essential for HDP1's function
319 remains unclear. Similarly, identifying interactions with other nuclear proteins and
320 genomic locations will offer important insights into its function. Of particular interest will
321 be whether HDP1 regulates gene expression by altering chromatin structure or is more
322 directly involved in the recruitment of RNA polymerase.

323 MATERIALS & METHODS

324 Parasite culture

325 Unless otherwise noted, parasite strains were grown in 0.5% AlbuMAX II supplemented malaria
326 complete medium using stablished cell culture techniques (Moll et al., 2008) at 3% hematocrit
327 and below 3% parasitemia. Strains expressing selectable markers were maintained under
328 constant drug-selection. Toxoplasma tachyzoites were cultured as described in (Morlon-Guyot et
329 al., 2018).

330 Gametocyte induction

331 Gametocytes were induced synchronously as previously described in (Poran et al., 2017).
332 Gametocyte maturation was monitored by Giemsa-stained thin blood smears and gametocytemia
333 was counted on the fifth day of development. The gametocyte commitment rate was calculated
334 by dividing the day 5 gametocytemia by the day 1 parasitemia, counted before addition of N-
335 acetyl-D-glucosamine. Gametocytes were purified from culture at the required development stage
336 using magnetic columns (LS columns, Miltenyi Biotec). For knockdown experiments in the HDP1-
337 glmS line, at the gametoring stage and either 5 mM glucosamine or solvent control was added.

338 **Generation of transgenic strains**

339 Transfection of ring-stage parasites were performed as previously described (Rug and Maier,
340 2012) and selected on 4nM WR99210 and 1.5 µM DSM1 for two weeks. To obtain Δ*hdp1*
341 parasites, selection with WR99210 was kept all the time. Genome editing was performed by
342 CRISR/Cas9 technology using the system described by (Ghorbal et al., 2014). The pL6-DX2
343 plasmid, containing the sgRNA-expression cassette and the positive selectable marker cassette
344 (*cam* promoter-*hdhfr*-*hrp2*/ts 3'*utr*) was used as backbone. Homology boxes were PCR amplified
345 from NF54 genomic DNA, using specific primers flanked by appropriate overlapping region from
346 pL6-DX2 plasmid (list of primers, see Supplementary Table) that allowed the cloning by Gibson
347 assembly. All PCR reactions were set using Advantage Genomic LA polymerase (Takara, Cat.
348 N° 639152). *Plasmodium* codon optimized sequences for HALO-tag and triple Ty1 epitope tag
349 were synthetized as gene-Blocks (Genewiz). PCR products were purified from agarose gel using
350 the Zymoclean Gel DNA Recovery Kit (Zymo Research, Cat. N° D4008). Homology boxes were
351 cloned through *AflII* and *SpeI* cutting sites, while annealed oligonucleotides paired encoding
352 sgRNA with targeting sequence (Table) were inserted through the *XhoI* site, placed upstream of
353 the sgRNA scaffold sequence. Sanger sequencing confirmed the absence of undesired mutations
354 in the homology boxes and the sgRNA. Genomic DNA from transfectant parasites was isolated
355 with QIAamp DNA blood Kit (Qiagen, Cat. N° 51106) and diagnostic PCR's were set using Taq
356 phusion DNA polymerase (Invitrogen). The TGME49_233160-HA parasite line was generated as
357 part of an earlier study by tagging of the endogenous locus in the *T. gondii* RH-ku80ko strain as
358 described in (Morlon-Guyot et al., 2018).

359 **Flow cytometric analysis of gametocyte viability**

360 Gametocytes were stained with 16 µM Hoechst33342 and 50 nM DilC1 for 30min at 37˚C. Using
361 a Cytek DxP12 flow cytometer, gametocytemia was determined by gating for DNA-positive,
362 hemozoin-high cells and gametocyte viability was inferred based on mitochondrial membrane

363 potential dependent accumulation of DilC1(5) for 1000 gametocytes (Tanaka and Williamson,
364 2011).

365 **Nuclear extract preparation and high salt fractionation**

366 Nuclear enriched fraction was prepared following the protocol previously described in (Flueck et
367 al., 2009), with some modifications. Briefly, parasites released from RBC's by saponin treatment
368 (0.01%) were lysed with ice-chilled CLB (20mM HEPES pH 7.9; 10mM KCl; 1mM EDTA pH 8.0;
369 1mM EGTA pH 8.0; 0.65% NP-40; 1mM DTT, 1x Roche Complete protease inhibitors cocktail).
370 Nuclei were pelleted at 3,000 x *g* for 20min at 4ºC and cytoplasmic fraction was removed. Nuclei
371 were resuspended in digestion buffer (20mM Tris- HCl, pH 7.5, 15mM NaCl, 60mM KCl, 1mM
372 $CaCl_2$, 5mM $MgCl_2$, 300mM sucrose, 0.4% NP-40, 1mM DTT, 1x Roche Complete protease
373 inhibitors cocktail EDTA-free) and treated with 5U of micrococcal nuclease (ThermoFisher, Cat.
374 Nº 88216) for 30 min in a water bath at 37ºC. Soluble and insoluble nuclear fractions were
375 recovered by centrifugation at 3,000 x *g* for 10 min at 4º C. Insoluble nuclear fraction were treated
376 with salt fractionation buffer (10mM Tris HCl pH 7.4; 2mM $MgCl_2$; 2mM EGTA pH 8.0; 0.1% Triton
377 X-100; 0.1mM PMSF; 1x Roche Complete protease inhibitors cocktail) supplemented with
378 increasing NaCl concentrations (80-600mM) while rotating at 4ºC for 30 min. All supernatants
379 were recovered by centrifugation at 700 x *g* for 4 min at 4ºC and last remaining pellet was
380 resuspended in 1x PBS supplemented with protease inhibitors cocktail. 5% of each fraction was
381 prepared for Western blotting in order to check quality of fractionation.

382 **Immunoblotting**

383 For SDS-PAGE, total protein lysates were prepared using saponin-lysed parasites resuspended
384 with 1x Laemmli loading buffer diluted in 1x PBS supplemented with 1x Roche Complete protease
385 inhibitors cocktail. Protein samples were separated in 4-15% polyacrylamide gels and transferred
386 to 0.2 µm Immobilion-P^{SQ} transfer membrane (Millipore, Cat. No ISEQ00010) using a Bio-Rad
387 transfer system. Membranes were blocked in 5% skim milk/1x TBS-Tween20 for 1 hour at RT.
388 Primary and secondary antibodies were prepared in 3% skim milk/1x TBS-Tween20 and
389 incubated for 1 hour at RT. Membranes were washed four times with 1x TBS-Tween20 for 10
390 min, after primary and secondary antibody incubations. The following primary antibodies were
391 used in this study: Anti-Ty1 BB2 mouse (1:2,500; Invitrogen Cat. Nº MA5-23513), anti-PhIL1 rabbit
392 (1:5,000 (Saini et al., 2017)), anti-PfHsp70 rabbit (1:5,000; StreesMarq Biosciences Cat. Nº SPC-
393 186D), anti-Histone 4 rabbit (1:2,000; Diagenode Cat. Nº C15410156-50). HRP-conjugated anti-
394 mouse and anti-rabbit antibodies were used (1:5,000, Millipore). Immunoblots were incubated
395 with the chemiluminescent substrate SuperSignal West Pico PLUS (ThermoFisher, Cat. Nº

396 34578) following manufacturer directions. Images were obtained using Azure c300 digital imaging
397 system (Azure Biosystems).

398 **Live-cell and Immunofluorescence microscopy**

399 For live-cell microscopy of *hdp1-gfp* and NF54 gametocytes, infected red blood cells were stained
400 with 16 µM Hoechst33342 in incomplete media for 15 min at 37° C and imaged at 1000×
401 magnification using a Leica DMI6000 microscope with differential interference contrast bright field
402 optics, DAPI, and GFP filter cubes with identical exposure times.

403 For immunofluorescence microscopy of *hdp1-Ty1* and *hdp1-glmS* gametocytes, cells were
404 seeded onto slides with Concanavilin A (5mg/ml; Sigma) as described in (Mehnert et al., 2019),
405 then fixed with a solution of 4% paraformaldehyde/0.0075% glutaraldehyde for 20 min at 37° C.
406 Parasites were permeabilized with 0.1% Triton X-100 for 15 min at RT followed by blocking with
407 3% BSA. Primary antibodies (anti-Ty1 BB2 mouse 1:1,000; anti-PhiL1 rabbit 1:400) were allowed
408 to bind for 1 hour in 3% BSA/PBS followed by three washes with blocking buffer for 5 min.
409 Secondary antibodies diluted 1:500 (anti-mouse-Alexa546 and anti-rabbit-Alexa488, Invitrogen)
410 plus 16 µM Hoechst33342 were added in fresh blocking buffer and incubated for 1 hour. Z-stacks
411 of stained specimens were collected at 1000× magnification using a Leica DMI6000 microscope
412 with differential interference contrast bright field optics, DAPI, and RFP filter cubes with identical
413 exposure times. Fluorescent channel z-stacks were deconvolved using the ImageJ
414 DeconvolutionLab2 plugin (NLLS algorithm) followed by maximum intensity z-projection and
415 background adjustment. Immunofluorescence microscopy of Toxoplasma tachyzoites was carries
416 out as previously described (Morlon-Guyot et al., 2018).

417 **Protein Expression and Purification**

418 Expression of recombinant HDP1-DBD motif was done using the Glutathione S-transferase (GST)
419 gene fusion system (GE, Healthcare). The pGEX-4T-1 (Addgene Cat. N° 27458001) plasmid was
420 used as backbone for cloning the codon optimized sequence comprising the last 87aa of HDP1.
421 Plasmid pGEX-GST-HDP1-DBD was transformed into BL21 (DE3) competent *E. coli* strain (NEB,
422 Cat. N^{o} C2527) and protein expression was done following the manufacturer directions with some
423 modifications. Briefly, an overnight culture was inoculated with one bacterial colony in 2x YT
424 media supplemented with the corresponding antibiotic. Next day, culture was diluted 1:100 with
425 fresh media and kept at 30° C with vigorous agitation. Bacterial growth was monitored until culture
426 reach exponential phase. At this point, IPTG (1mM final concentration) was added and the culture
427 was kept for another 2 hours at 30° C with vigorous agitation. Cells were harvested and

428 resuspended in lysis buffer (50mM Tris HCl pH 7.5; 100mM NaCl; 1mM DTT; 5% Glycerol; 1mM
429 PMSF; 1mM EDTA; 1x protease inhibitors cocktail) supplemented with Lysozyme (1mg/ml,
430 Sigma). In order to remove bacterial DNA from our putative DNA binding protein, lysate was
431 treated with polyethyleneimine (PEI) (0.1% v/v) (RR, 1991). Lysate was sonicated, cleared by
432 centrifugation at 14,000 x *g* for 30 min at 4º C. Protein extract was recovered and GST-HDP1-
433 DBD protein was purified using Pierce GST Spin purification kit (Cat. Nº 16106) following
434 manufacturer directions. Protein of interest was dialyzed using Slide-A-Lyzer Dialysis Cassette
435 10,000 MWCO (ThermoScientific, Cat. Nº 66810) and concentrated using Amicon Ultra
436 Centrifugal filters 10,000 MWCO (Millipore, Cat. Nº UFC901024). Purity was verified by
437 Coomassie staining after SDS-PAGE and concentration was measured by Bradford assay.

438 Sequence encoding HDP1 aa2991-3078 were cloned into the MCS1 of the pRSFDuet-1 vector
439 (Novagen) engineered with an N-terminal His-SUMO tag. The proteins were expressed in *E. coli*
440 strain BL21 CodonPlus(DE3)-RIL (Stratagene). Bacteria were grown in Luria-Bertani medium at
441 37°C to OD600=0.8 and induced with 0.4 mM IPTG at 18°C overnight. Cells were collected via
442 centrifugation at 5000×g and lysed via sonication in Lysis Buffer (20 mM Tris-HCl, pH 8.0, 500
443 mM NaCl, 20 mM imidazole, and 5% Glycerol) supplemented with 1 mM phenylmethylsulfonyl
444 fluoride and 0.5% Triton X-100. Cellular debris was removed by centrifugation at 20,000×g, and
445 the supernatant was loaded onto 5 ml HisTrap FF column (GE Healthcare) and eluted using the
446 lysis buffer supplemented with 500 mM imidazole. The elution was dialyzed at 4°C overnight
447 against the buffer (20 mM Tris-HCl, pH 8.0, 300 mM NaCl, 20 mM imidazole, and 5 mM β-
448 mercaptoethanol) with ULP1 protease added (lab stock). The sample was reloaded on the
449 HisTrap FF column to remove the His-SUMO tag. The flow-through was loaded on the Heparin
450 column (GE Healthcare) and eluted with a gradient of NaCl from 300 mM to 1 M. The target
451 protein was further purified by size exclusion chromatography (Superdex 200 [16/60], GE
452 Healthcare) in the buffer (20 mM Tris-HCl, pH 7.5, 200 mM NaCl, 1 mM MgCl2, and 1 mM DTT).
453 The high purity eluting fractions were detected by SDS-PAGE and concentrated to around 20
454 mg/ml. The protein was flash-frozen in liquid nitrogen and stored at -80°C.

455 **Protein Binding Microarray**

456 All GST-HDP1-DBD binding was analyzed twice in the PBMs. The PBM experiments were
457 performed as previously described (Berger and Bulyk, 2009; Berger et al., 2006). Briefly, custom
458 designed oligonucleotide arrays are double-stranded using a universal primer, incubated with
459 GST-HDP1-DBD fusion proteins, visualized with Alexa-488 conjugated anti-GST antibody, and
460 scanned using an Axon 4200A scanner. Proteins were used at the maximum concentration

461 obtained from purification and represent one-fifth of the total reaction volume used on the PBM.
462 In this study three different universal platforms were used covering all contiguous 8-mers as well
463 as gapped 8-mers spanning up to 10 positions. After data normalization and calculation of
464 enrichment scores the “Seed-and-Wobble” algorithm was applied to combine the data from two
465 separate experiments and create position weight matrices (PWMs). An enrichment score cut-off
466 of 0.45 was used to distinguish high affinity binding data from low affinity and non-specific binding.
467 The score for each 8-mer reflects the affinity of a DNA binding domain for that sequence, with
468 higher scores representing tighter interactions. Secondary motifs were identified by running the
469 “rerank” program until E-scores below 0.45 were obtained. The PBM analysis suite was
470 downloaded from the_brain.bwh.harvard.edu/PBMAnalysisSuite/index.html.

471 **Isothermal Titration Calorimetry**

472 All the binding experiments were performed on a Microcal ITC 200 calorimeter. Purified HLH
473 proteins were dialyzed overnight against the buffer (20 mM HEPES, pH 7.5, 150 mM NaCl, 1 mM
474 DTT) at 4°C. DNA oligos were synthesized by Integrated DNA Technologies (IDT) and dissolved
475 in the same buffer. The assays perform with 1 mM DNA duplexes containing the tandem motif
476 (TAGTGCACCTATGGTGCACTT) with 0.1 mM HLH90 proteins. Each reaction's exothermic heat
477 was measured by sequential injection of the 2 μL DNA duplexes into proteins solution, spaced at
478 intervals of 180 seconds. The titration was according to standard protocol at 20°C and the data
479 were fitted using the program Origin 7.0.

480 **Gel-shift Assays**

481 Electrophoretic mobility shift assays were performed using Light Shift EMSA kits (Thermo
482 Scientific) using 24 pg of protein and 40 fmol of probe, as previously described (Campbell et al.,
483 2010). Biotinylated double-stranded probes were generated with the indicated sequence.

484 **RNA Extraction, cDNA synthesis, and quantitative RT-PCR**

485 Total RNA from saponin-lysed parasites was extracted using Trizol (Invitgrogen) and Direct-Zol
486 RNA MiniPrep Plus kit (Zymo Research). The cDNA was prepared from 100-500ng total RNA
487 (pre-treated with 2U DNase I, amplification grade) using SuperScript III Reverse Transcriptase kit
488 (Invitrogen) and random hexamers. Quantitative PCR was performed on the Quant Studio 6 Flex
489 (Thermo Fisher) using iTaq Sybr Green (Bio-Rad) with specific primers for selected target genes
490 (Table). Quantities were normalized to seryl-tRNA synthetase (PF3D7_0717700). Analysis of

491 expression of the *var* gene family was performed by using the primer set described in Salanti et
492 al. 2003 (Salanti et al., 2003).

493 **RNA sequencing**

494 Following gametocyte induction, highly synchronous cultures containing committed schizonts
495 were added to fresh RBCs and allowed to reinvade for 12 hours prior to the addition of 50mM N-
496 acetyl glucosamine to block the development of hemozoin-containing asexual trophozoites. On
497 day 2 of gametocyte development, stage I gametocytes were purified magnetically and total RNA
498 was extracted as described above. Following RNA isolation, total RNA integrity was checked
499 using a 2100 Bioanalyzer (Agilent Technologies, Santa Clara, CA). RNA concentrations were
500 measured using the NanoDrop system (Thermo Fisher Scientific, Inc., Waltham, MA). Preparation
501 of RNA sample library and RNA-seq were performed by the Genomics Core Laboratory at Weill
502 Cornell Medicine. rRNA was removed from Total RNA using Illumina Ribo Zero Gold for
503 human/mouse/rat kit. Using Illumina TruSeq RNA Sample Library Preparation v2 kit (Illumina,
504 San Diego, CA), Messenger RNA was fragmented into small pieces using divalent cations under
505 elevated temperature. The cleaved RNA fragments were copied into first strand cDNA using
506 reverse transcriptase and random primers. Second strand cDNA synthesis followed, using DNA
507 Polymerase I and RNase H. The cDNA fragments then went through an end repair process, the
508 addition of a single 'A' base, and then ligation of the adapters. The products were then purified
509 and enriched with PCR to create the final cDNA library. were pooled and sequenced on Illumina
510 HiSeq4000 sequencer with single-end 50 cycles. Read files were checked for quality by using
511 FASTQC (https://github.com/s-andrews/FastQC). Reads were trimmed to remove low-quality
512 positions and adapter sequences using cutadapt (version 1.16) (Martin, 2011). Reads were
513 mapped against the *P. falciparum* 3D7 reference genome v.40 (Warrenfeltz et al., 2018) using
514 STAR aligner (version 2.61) (Dobin et al., 2012) and nuclear-encoded genes were analyzed for
515 differential gene expression using cufflinks (version 2.2.1) (Trapnell et al., 2013). Genes with a
516 false discovery rate of <=0.05 with a mean FPKM >5 in at least one strain were called significant.
517 For genes with FPKM > 5 in one strain and no detectable expression in the other, FKPM values
518 were set to 0.1 for purposes of fold-change calculation. Gene Set Enrichment Analysis was
519 carried out with the FGSEA Bioconductor package (Korotkevich et al., 2019) with a false discovery
520 cutoff of <=0.05.

521 **Hi-C Sequencing**

522 Parasites were crosslinked in 1.25% formaldehyde in warm PBS for 25 min on a rocking platform.
523 Glycine was added to a final concentration of 150 mM, followed by 15 min of incubation at 37°C
524 and 15 min of incubation at 4°C. The parasites were centrifuged at 660g for 20 min at 4 °C,
525 resuspended in 5 volumes of ice-cold PBS, and incubated for 10 min at 4°C. Parasites were
526 centrifuged at 660g for 15 min at 4°C, washed once in ice-cold PBS, and stored as a pellet at
527 −80°C. Parasite pellets were then thawed on ice in Hi-C lysis buffer (10 mM Tris-HCl at pH8.0,
528 10 mM NaCl, 2 mM AEBSF, Roche Complete Mini EDTA-free protease inhibitor cocktail,0.25%
529 Igepal CA-630). Parasite membranes were disrupted by passing the lysate through a 26.5- gauge
530 needle 15 times with a syringe. Samples were spun and pellets were washed once with ice-cold
531 Hi-C lysis buffer, resuspended in 0.5% SDS and incubated at 62°C for 10 min to solubilize the
532 chromatin. The SDS was neutralized by the addition of nuclease-free water and 1% Triton X-100,
533 for 15-minutes at 37°C. DNA was then digested using MboI restriction overnight at 37°C. After
534 digestion, the enzyme was heat inactivated at 62°C for 20 min, and then cooled to RT. 5'
535 overhangs were filled in by Biotin-14-dCTP (Invitrogen) using DNA Polymerase I and Large
536 (Klenow) Fragment (NEB) for 45 min at 37°C. Blunt-end ligation was performed using T4 DNA
537 Ligase at 20°C for 4 hours. The nuclei were spun down to remove random ligation products and
538 to reduce the overall reaction volume and resuspend in decrosslinking buffer (50 mM Tris-HCl,
539 pH 8.0, 1% SDS, 1 mM EDTA, 500 mM NaCl) before adding RNaseA (20 mg/ml) for 45 min at
540 37°C and proteinase K (NEB) treatment overnight at 45°C. DNA was extracted using Agencourt
541 AMPure XP beads (Beckman Coulter) and eluted in 10 mM Tris-HCl at pH 8.0. The purified DNA
542 was sheared on a Covaris S220 and biotinylated DNA fragments were pull-down using MyOne
543 Streptavidin T1 magnetic beads (Invitrogen) at 55°C for 2 min, washed and resuspended in T4
544 DNA Ligase Buffer to perform end-repair on DNA fragments bound to the beads containing DNA
545 Polymerase I, Large (Klenow) Fragment (NEB), and T4 DNA Polymerase (NEB) and incubated
546 for 30 min at 20°C. The beads were washed twice before performing A-tailing using Klenow
547 Fragment (3´→5´ exo–nuclease) (NEB)) for 30 min at 37°C. The beads were then washed twice
548 and resuspended in T4 DNA Ligase Buffer to perform adapter ligation using the NEBNext Illumina
549 Adapter for 15 min at 20°C in a thermomixer. The beads were then resuspended in 100 µl of 10
550 mM Tris-HCl at pH 8.0 and transferred to a new tube to amplify the library using the HiFi HotStart
551 ReadyMix (KAPA Biosystems) as well as the universal forward primer and barcoded reverse
552 primer before being incubated with the following PCR program: 45 sec at 98°C, 12 cycles of 15
553 sec at 98°C, 30 sec at 55°C, 30 sec at 62°C and a final extension of 5 min at 62°C. The library
554 was then purified using double-SPRI size selection, with 0.5Å~ right-side selection (25 µl AMPure
555 XP beads) and 1.0Å~ left-side selection (25 µl AMPure XP beads). Libraries were quantified by

556 NanoDrop (Thermo Scientific) and Bioanalyzer (Agilent), prior to multiplexing and sequencing in
557 a 75-bp paired-end run on a NextSeq500 (Illumina).

558 **Analysis of Hi-C Data**

559 Bed files of virtual MboI (GATC) digest of the *P. falciparum* genome were generated with
560 digest_genome.py from the HiC-Pro suite (Servant et al., 2015). The paired-end reads were
561 processed (i.e. mapped, paired, and de-duplicated), binned at 10kb resolution, and normalized
562 using the ICE algorithm using HiC-Pro. Reproducibility and strain-dependent differences (Figure
563 6A) between Hi-C samples was evaluated by correlation analysis using HiCSpector (Yan et al.,
564 2017) and GenomeDISCO (Ursu et al., 2018). Interaction maps (Figure S7) were generated by
565 plotting intra-chromosomal ICE-normalized interactions. Summary statistics (Figure 6B) of intra-
566 chromosomal interaction distances were calculated for each strain and chromosome from
567 normalized ICE interaction counts using R. Differential interaction analysis was carried out at 10
568 kb resolution for each replicate using selfish (Ardakany et al., 2019) based on ICE-normalized
569 interaction counts from the Hi-C Pro all-valid-pairs matrix and reformatted into the ".hic" file-format
570 using Juicebox (Robinson et al., 2018). All genome-wide bin pairs with significant changes in
571 interaction frequency between the *hdp1*-ty1 and Δ*hdp1* strains with a FDR <=0.1 in both replicate
572 pairs are shown in the top left of Figure 6C. For the analysis of chromosome-end interactions,
573 interactions fold-change were calculated for all interactions in bins between the chromosome end
574 and the first protein coding gene. As the final bin on each chromosome varies in size, an additional
575 bin was added for ends truncated by telomere healing (5R, 11R, and 14R) to ensure interaction
576 counts were calculated for at least 10kb.

577 **ACKNOWLEDGEMENTS**

578 We wish to thank Dr. Pawan Malhotra for the generous gift of anti-PhIL1 antibodies, V. Carruthers
579 for the generous gift of anti-Ty1 antibodies, the Weill Cornell Medicine genomics core for technical
580 support, M. Llinas and R. Bartfai for separate HDP1 ChIP-seq attempts with *hdp1*-gfp and *hdp1*-
581 ty1 gametocytes, respectively, as well as K. Deitsch and J. King for valuable feedback on the
582 manuscript. This work was supported by startup funds from Weill Cornell Medicine (BK), NIAID
583 1R01AI141965 (BK), 1R01 AI125565 (ML), 1R01 AI136511 (KLR), R21 AI142506-01 (KLR), the
584 University of California, Riverside (NIFA-Hatch-225935-KLR), and support from the Mathers
585 Foundation (DJP).

586 **AUTHOR CONTRIBUTIONS**

Conceptualization: B.F.C.K.; Methodology: B.F.C.K., R.C.M., W.X., W.N., K.G.L.; Investigation: R.C.M., X.T., W.X.,T.L.,G.B., L.O., W.D.; Software, Formal Analysis, Data Curation: B.F.C.K., T.L.; Writing – Original Draft: R.C.M.; Writing –Review & Editing: B.F.C.K., R.C.M.; Visualization: R.C.M., B.F.C.K.; Supervision: B.F.C.K., K.G.L., M.L., W.N, D.P., Project Administration: B.F.C.K; Funding Acquisition: B.F.C.K.;

DECLARATIONS OF INTEREST

The authors declare no competing interests.

595 **REFERENCES**

596 Ardakany, A.R., Ay, F., Lonardi, S., 2019. Selfish: discovery of differential chromatin interactions via a
597 self-similarity measure. Bioinformatics 35, i145–i153. doi:10.1093/bioinformatics/btz362
598
599 Balaji, S., Babu, M.M., Iyer, L.M., Aravind, L., 2005. Discovery of the principal specific transcription factors
600 of Apicomplexa and their implication for the evolution of the AP2-integrase DNA binding domains.
601 Nucleic Acids Res 33, 3994–4006. doi:10.1093/nar/gki709
602
603 Bancells, C., Llorà-Batlle, O., Poran, A., Nötzel, C., Rovira-Graells, N., Elemento, O., Kafsack, B.F.C.,
604 Cortés, A., 2019. Revisiting the initial steps of sexual development in the malaria parasite Plasmodium
605 falciparum. Nat. Microbiol 4, 144–154. doi:10.1038/s41564-018-0291-7
606
607 Berger, M.F., Bulyk, M.L., 2009. Universal protein-binding microarrays for the comprehensive
608 characterization of the DNA-binding specificities of transcription factors. Nature Protocols 4, 393–411.
609 doi:10.1038/nprot.2008.195
610
611 Berger, M.F., Philippakis, A.A., Qureshi, A.M., He, F.S., Estep, P.W., Bulyk, M.L., 2006. Compact,
612 universal DNA microarrays to comprehensively determine transcription-factor binding site specificities.
613 Nat Biotechnol 24, 1429–1435. doi:10.1038/nbt1246
614
615 Bhattacharya, S., Conolly, R.B., Kaminski, N.E., Thomas, R.S., Andersen, M.E., Zhang, Q., 2010. A
616 Bistable Switch Underlying B-Cell Differentiation and Its Disruption by the Environmental Contaminant
617 2,3,7,8-Tetrachlorodibenzo-p-dioxin. Toxicol Sci 115, 51–65. doi:10.1093/toxsci/kfq035
618
619 Brancucci, N.M.B., Bertschi, N.L., Zhu, L., Niederwieser, I., Chin, W.H., Wampfler, R., Freymond, C.,
620 Rottmann, M., Felger, I., Bozdech, Z., Voss, T.S., 2014. Heterochromatin protein 1 secures survival
621 and transmission of malaria parasites. Cell Host Microbe 16, 165–176.
622 doi:10.1016/j.chom.2014.07.004
623
624 Bunnik, E.M., Cook, K.B., Varoquaux, N., Batugedara, G., Prudhomme, J., Cort, A., Shi, L., Andolina, C.,
625 Ross, L.S., Brady, D., Fidock, D.A., Nosten, F., Tewari, R., Sinnis, P., Ay, F., Vert, J.-P., Noble, W.S.,
626 Le Roch, K.G., 2018. Changes in genome organization of parasite-specific gene families during the
627 Plasmodium transmission stages. Nature Communications 9, 1910. doi:10.1038/s41467-018-04295-5
628
629 Bürglin, T.R., Affolter, M., 2016. Homeodomain proteins: an update. Chromosoma 125, 497–521.
630 doi:10.1007/s00412-015-0543-8
631
632 Calhoun, S.F., Reed, J., Alexander, N., Mason, C.E., Deitsch, K.W., Kirkman, L.A., Boyle, J.P., 2017.
633 Chromosome End Repair and Genome Stability in Plasmodium falciparum. mBio 8, e00547–17.
634 doi:10.1128/mBio.00547-17
635
636 Campbell, T.L., De Silva, E.K., Olszewski, K.L., Elemento, O., Llinás, M., 2010. Identification and
637 genome-wide prediction of DNA binding specificities for the ApiAP2 family of regulators from the
638 malaria parasite. PLoS Pathog 6, e1001165. doi:10.1371/journal.ppat.1001165
639
640 Coleman, B.I., Skillman, K.M., Jiang, R.H.Y., Childs, L.M., Altenhofen, L.M., Ganter, M., Leung, Y.,
641 Goldowitz, I., Kafsack, B.F.C., Marti, M., Llinás, M., Buckee, C.O., Duraisingh, M.T., 2014. A
642 Plasmodium falciparum Histone Deacetylase Regulates Antigenic Variation and Gametocyte
643 Conversion. Cell Host Microbe 16, 177–186. doi:10.1016/j.chom.2014.06.014
644
645 Dobin, A., Davis, C.A., Schlesinger, F., Drenkow, J., Zaleski, C., Jha, S., Batut, P., Chaisson, M.,
646 Gingeras, T.R., 2012. STAR: ultrafast universal RNA-seq aligner. Bioinformatics 29, 15–21.
647 doi:10.1093/bioinformatics/bts635
648

649 Filarsky, M., Fraschka, S.A., Niederwieser, I., Brancucci, N.M.B., Carrington, E., Carrió, E., Moes, S.,
650 Jenoe, P., Bartfai, R., Voss, T.S., 2018. GDV1 induces sexual commitment of malaria parasites by
651 antagonizing HP1-dependent gene silencing. Science 359, 1259–1263. doi:10.1126/science.aan6042
652
653 Flueck, C., Bartfai, R., Niederwieser, I., Witmer, K., Alako, B.T.F., Moes, S., Bozdech, Z., Jenoe, P.,
654 Stunnenberg, H.G., Voss, T.S., 2010. A major role for the Plasmodium falciparum ApiAP2 protein
655 PfSIP2 in chromosome end biology. PLoS Pathog 6, e1000784. doi:10.1371/journal.ppat.1000784
656
657 Flueck, C., Bartfai, R., Volz, J., Niederwieser, I., Salcedo-Amaya, A.M., Alako, B.T.F., Ehlgen, F., Ralph,
658 S.A., Cowman, A.F., Bozdech, Z., Stunnenberg, H.G., Voss, T.S., 2009. Plasmodium falciparum
659 Heterochromatin Protein 1 Marks Genomic Loci Linked to Phenotypic Variation of Exported Virulence
660 Factors. PLoS Pathog 5, e1000569. doi:10.1371/journal.ppat.1000569
661
662 Fraschka, S.A., Filarsky, M., Hoo, R., Niederwieser, I., Yam, X.Y., Brancucci, N.M.B., Mohring, F.,
663 Mushunje, A.T., Huang, X., Christensen, P.R., Nosten, F., Bozdech, Z., Russell, B., Moon, R.W., Marti,
664 M., Preiser, P.R., Bartfai, R., Voss, T.S., 2018. Comparative Heterochromatin Profiling Reveals
665 Conserved and Unique Epigenome Signatures Linked to Adaptation and Development of Malaria
666 Parasites. Cell Host Microbe 23, 407–420.e8. doi:10.1016/j.chom.2018.01.008
667
668 Ghorbal, M., Gorman, M., Macpherson, C.R., Martins, R.M., Scherf, A., Lopez-Rubio, J.J., 2014. Genome
669 editing in the human malaria parasite Plasmodium falciparum using the CRISPR-Cas9 system. Nat
670 Biotechnol 32, 819–821. doi:10.1038/nbt.2925
671
672 Hedgethorne, K., Eustermann, S., Yang, J.-C., Ogden, T.E.H., Neuhaus, D., Bloomfield, G., 2017.
673 Homeodomain-like DNA binding proteins control the haploid-to-diploid transition in Dictyostelium.
674 Science advances 3, e1602937. doi:10.1126/sciadv.1602937
675
676 Morlon-Guyot, J., El Hajj, H., Martin, K., Fols, A., Carillo, A., Berry, L., Burchmore, R., Meissner, M.,
677 Lebrun, M., Daher, W., 2018. A proteomic analysis unravels novel CORVET and HOPS proteins
678 involved in Toxoplasma gondii secretory organelles biogenesis. Cell Microbiol 20, e12870.
679 doi:10.1111/cmi.12870
680
681 Josling, G.A., Russell, T.J., Venezia, J., Orchard, L., van Biljon, R., Painter, H.J., Llinás, M., 2020.
682 Dissecting the role of PfAP2-G in malaria gametocytogenesis. Nature Communications 11, 1–13.
683 doi:10.1038/s41467-020-15026-0
684
685 Kafsack, B.F.C., Rovira-Graells, N., Clark, T.G., Bancells, C., Crowley, V.M., Campino, S.G., Williams,
686 A.E., Drought, L.G., Kwiatkowski, D.P., Baker, D.A., Cortés, A., Llinás, M., 2014. A transcriptional
687 switch underlies commitment to sexual development in malaria parasites. Nature 507, 248–252.
688 doi:10.1038/nature12920
689
690 Kent, R.S., Modrzynska, K.K., Cameron, R., Philip, N., Billker, O., Waters, A.P., 2018. Inducible
691 developmental reprogramming redefines commitment to sexual development in the malaria parasite
692 Plasmodium berghei. Nat. Microbiol 3, 1206–1213. doi:10.1038/s41564-018-0223-6
693
694 Korotkevich, G., Sukhov, V., Sergushichev, A., 2019. Fast gene set enrichment analysis. bioRxiv 10,
695 060012. doi:10.1101/060012
696
697 Lopez-Rubio, J.J., Mancio-Silva, L., Scherf, A., 2009. Genome-wide analysis of heterochromatin
698 associates clonally variant gene regulation with perinuclear repressive centers in malaria parasites.
699 Cell Host Microbe 5, 179–190. doi:10.1016/j.chom.2008.12.012
700
701 Martin, M., 2011. Cutadapt removes adapter sequences from high-throughput sequencing reads.
702 EMBnet.journal 17, 10–12.
703

704 Mehnert, A.-K., Simon, C.S., Guizetti, J., 2019. Immunofluorescence staining protocol for STED
705 nanoscopy of Plasmodium-infected red blood cells. Mol Biochem Parasitol 229, 47–52.
706 doi:10.1016/j.molbiopara.2019.02.007
707
708 Modrzynska, K., Pfander, C., Chappell, L., Yu, L., Suarez, C., Dundas, K., Gomes, A.R., Goulding, D.,
709 Rayner, J.C., Choudhary, J., Billker, O., 2017. A Knockout Screen of ApiAP2 Genes Reveals Networks
710 of Interacting Transcriptional Regulators Controlling the Plasmodium Life Cycle. Cell Host Microbe 21,
711 11–22. doi:10.1016/j.chom.2016.12.003
712
713 Moll, K., Ljungström, I., Perlmann, H., Scherf, A., 2008. Methods in malaria research.
714
715 Nixon, C.P., Nixon, C.E., Michelow, I.C., Silva-Viera, R.A., Colantuono, B., Obeidallah, A.S., Jha, A.,
716 Dockery, D., Raj, D., Park, S., Duffy, P.E., Kurtis, J.D., 2018. Antibodies to PfsEGXP, an Early
717 Gametocyte-Enriched Phosphoprotein, Predict Decreased Plasmodium falciparum Gametocyte
718 Density in Humans. J INFECT DIS 218, 1792–1801. doi:10.1093/infdis/jiy416
719
720 Norman, T.M., Lord, N.D., Paulsson, J., Losick, R., 2015. Stochastic Switching of Cell Fate in Microbes.
721 Annu Rev Microbiol 69, 381–403. doi:10.1146/annurev-micro-091213-112852
722
723 Painter, H.J., Carrasquilla, M., Llinás, M., 2017. Capturing in vivo RNA transcriptional dynamics from the
724 malaria parasite Plasmodium falciparum. Genome Res 27, 1074–1086. doi:10.1101/gr.217356.116
725
726 Park, B.O., Ahrends, R., Teruel, M.N., 2012. Consecutive Positive Feedback Loops Create a Bistable
727 Switch that Controls Preadipocyte-to-Adipocyte Conversion. Cell Reports 2, 976–990.
728 doi:10.1016/j.celrep.2012.08.038
729
730 Parkyn Schneider, M., Liu, B., Glock, P., Suttie, A., McHugh, E., Andrew, D., Batinovic, S., Williamson, N.,
731 Hanssen, E., McMillan, P., Hliscs, M., Tilley, L., Dixon, M.W.A., 2017. Disrupting assembly of the inner
732 membrane complex blocks Plasmodium falciparum sexual stage development. PLoS Pathog 13,
733 e1006659. doi:10.1371/journal.ppat.1006659
734
735 Poran, A., Nötzel, C., Aly, O., Mencia-Trinchant, N., Harris, C.T., Guzman, M.L., Hassane, D.C.,
736 Elemento, O., Kafsack, B.F.C., 2017. Single-cell RNA sequencing reveals a signature of sexual
737 commitment in malaria parasites. Nature 551, 95–99. doi:10.1038/nature24280
738
739 Pradhan, L., Genis, C., Scone, P., Weinberg, E.O., Kasahara, H., Nam, H.-J., 2012. Crystal Structure of
740 the Human NKX2.5 Homeodomain in Complex with DNA Target. Biochemistry 51, 6312–6319.
741 doi:10.1021/bi300849c
742
743 Prommana, P., Uthaipibull, C., Wongsombat, C., Kamchonwongpaisan, S., Yuthavong, Y., Knuepfer, E.,
744 Holder, A.A., Shaw, P.J., 2013. Inducible Knockdown of Plasmodium Gene Expression Using the glmS
745 Ribozyme. PLoS ONE 8, e73783. doi:10.1371/journal.pone.0073783
746
747 Robinson, J.T., Turner, D., Durand, N.C., Thorvaldsdóttir, H., Mesirov, J.P., Aiden, E.L., 2018. Juicebox.js
748 Provides a Cloud-Based Visualization System for Hi-C Data. cels 6, 256–258.e1.
749 doi:10.1016/j.cels.2018.01.001
750
751 RR, B., 1991. Use of polyethyleneimine in purification of DNA-binding proteins. Meth. Enzymol. 208, 3–
752 10. doi:10.1016/0076-6879(91)08003-z
753
754 Rug, M., Maier, A.G., 2012. Transfection of Plasmodium falciparum, in: Malaria, Methods in Molecular
755 Biology. Humana Press, Totowa, NJ, Totowa, NJ, pp. 75–98. doi:10.1007/978-1-62703-026-7_6
756
757 Warrenfeltz, S., Basenko, E.Y., Crouch, K., Harb, O.S., Kissinger, J.C., Roos, D.S., Shanmugasundram,
758 A., Silva-Franco, F, 2018. EuPathDB: The Eukaryotic Pathogen Genomics Database Resource.
759 Methods Mol Biol 1757, 69–113. doi:10.1007/978-1-4939-7737-6_5

Saini, E., Zeeshan, M., Brady, D., Pandey, R., Kaiser, G., Koreny, L., Kumar, P., Thakur, V., Tatiya, S., Katris, N.J., Limenitakis, R.S., Kaur, I., Green, J.L., Bottrill, A.R., Guttery, D.S., Waller, R.F., Heussler, V., Holder, A.A., Mohmmed, A., Malhotra, P., Tewari, R., 2017. Ph otosensitized I NA- L abelled protein 1 (PhIL1) is novel component of the inner membrane complex and is required for Plasmodium parasite development. Sci. Rep. 7, 15577. doi:10.1038/s41598-017-15781-z

Salanti, A., Staalsoe, T., Lavstsen, T., Jensen, A.T.R., Sowa, M.P.K., Arnot, D.E., Hviid, L., Theander, T.G., 2003. Selective upregulation of a single distinctly structured var gene in chondroitin sulphate A-adhering Plasmodium falciparum involved in pregnancy-associated malaria. Mol Microbiol 49, 179–191. doi:10.1046/j.1365-2958.2003.03570.x

Satory, D., Gordon, A.J., Halliday, J.A., Herman, C., 2011. Epigenetic switches: can infidelity govern fate in microbes? Curr Opin Microbiol 14, 212–217. doi:10.1016/j.mib.2010.12.004

Servant, N., Varoquaux, N., Lajoie, B.R., Viara, E., Chen, C.-J., Vert, J.-P., Heard, E., Dekker, J., Barillot, E., 2015. HiC-Pro: an optimized and flexible pipeline for Hi-C data processing. Genome Biol 16, 1–11. doi:10.1186/s13059-015-0831-x

Sinha, A., Hughes, K.R., Modrzynska, K.K., Otto, T.D., Pfander, C., Dickens, N.J., Religa, A.A., Bushell, E., Graham, A.L., Cameron, R., Kafsack, B.F.C., Williams, A.E., Llinás, M., Berriman, M., Billker, O., Waters, A.P., 2014. A cascade of DNA-binding proteins for sexual commitment and development in Plasmodium. Nature 507, 253–257. doi:10.1038/nature12970

Tanaka, T.Q., Williamson, K.C., 2011. A malaria gametocytocidal assay using oxidoreduction indicator, alamarBlue. Mol Biochem Parasitol 177, 160–163. doi:10.1016/j.molbiopara.2011.02.005

Tibúrcio, M., Silvestrini, F., Bertuccini, L., Sander, A.F., Turner, L., Lavstsen, T., Alano, P., 2013. Early gametocytes of the malaria parasite Plasmodium falciparum specifically remodel the adhesive properties of infected erythrocyte surface. Cell Microbiol 15, 647–659. doi:10.1111/cmi.12062

Trapnell, C., Hendrickson, D.G., Sauvageau, M., Goff, L., Rinn, J.L., Pachter, L., 2013. Differential analysis of gene regulation at transcript resolution with RNA-seq. Nat Biotechnol 31, 46–53. doi:10.1038/nbt.2450

Ursu, O., Boley, N., Taranova, M., Wang, Y.X.R., Yardimci, G.G., Stafford Noble, W., Kundaje, A., 2018. GenomeDISCO: a concordance score for chromosome conformation capture experiments using random walks on contact map graphs. Bioinformatics 34, 2701–2707. doi:10.1093/bioinformatics/bty164

van Biljon, R., van Wyk, R., Painter, H.J., Orchard, L., Reader, J., Niemand, J., Llinás, M., Birkholtz, L.-M., 2019. Hierarchical transcriptional control regulates Plasmodium falciparum sexual differentiation. BMC Genomics 20, 920. doi:10.1186/s12864-019-6322-9

Yan, K.-K., Yardımcı, G.G., Yan, C., Noble, W.S., Gerstein, M., 2017. HiC-spector: a matrix library for spectral and reproducibility analysis of Hi-C contact maps. Bioinformatics 33, 2199–2201. doi:10.1093/bioinformatics/btx152

Young, J.A., Fivelman, Q.L., Blair, P.L., la Vega, de, P., Le Roch, K.G., Zhou, Y., Carucci, D.J., Baker, D.A., Winzeler, E.A., 2005. The Plasmodium falciparum sexual development transcriptome: a microarray analysis using ontology-based pattern identification. Mol Biochem Parasitol 143, 67–79. doi:10.1016/j.molbiopara.2005.05.007

Yuda, M., Iwanaga, S., Kaneko, I., Kato, T., 2015. Global transcriptional repression: An initial and essential step for Plasmodium sexual development. Proceedings of the National Academy of Sciences. doi:10.1073/pnas.1504389112

816
817 Yuda, M., Kaneko, I., Iwanaga, S., Mura, Y., Kato, T., 2019. Female-specific gene regulation in malaria
818 parasites by an AP2-family transcription factor. Mol Microbiol 6, 1–51. doi:10.1111/mmi.14334
819
820 Zhang, C., Xiao, B., Jiang, Y., Zhao, Y., Li, Z., Gao, H., Ling, Y., Wei, J., Li, S., Lu, M., Su, X.-Z., Cui, H.,
821 Yuan, J., 2014. Systematic CRISPR-Cas9-Mediated Modifications of Plasmodium yoelii ApiAP2
822 Genes Reveal Functional Insights into Parasite Development. mBio 2017, 8 (6) e01986-17
823 doi:10.1128/mBio.01986-17

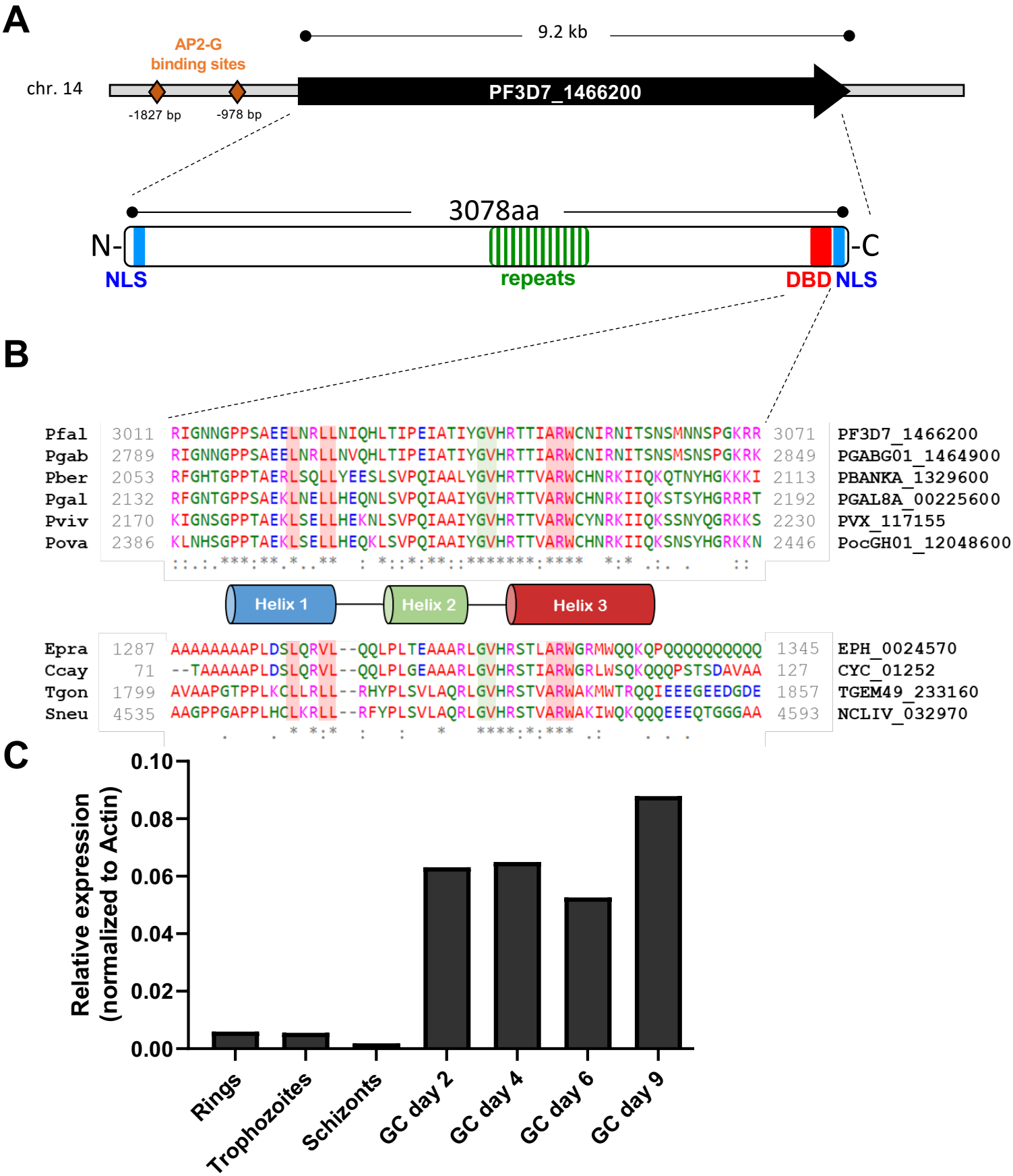

Figure 1: The predicted DNA-binding protein HDP1 is expressed in gametocytes. (A) The single exon locus Pf3D7_1466200 encodes a large 3078aa protein with a predicted C-terminal Helix-Turn-Helix DNA-binding domain (DBD) and two nuclear localization signals (NLS). Multiple AP2-G binding sites are located in the 2kb promoter region. **(B)** Alignment of the helix-turn-helix domain for homologs from other apicomplexan parasites. **(C)** Quantitative RT-PCR of *hdp1* transcripts found minimal expression in asexual blood stages with upregulation during gametocyte development. (mean of n=2).

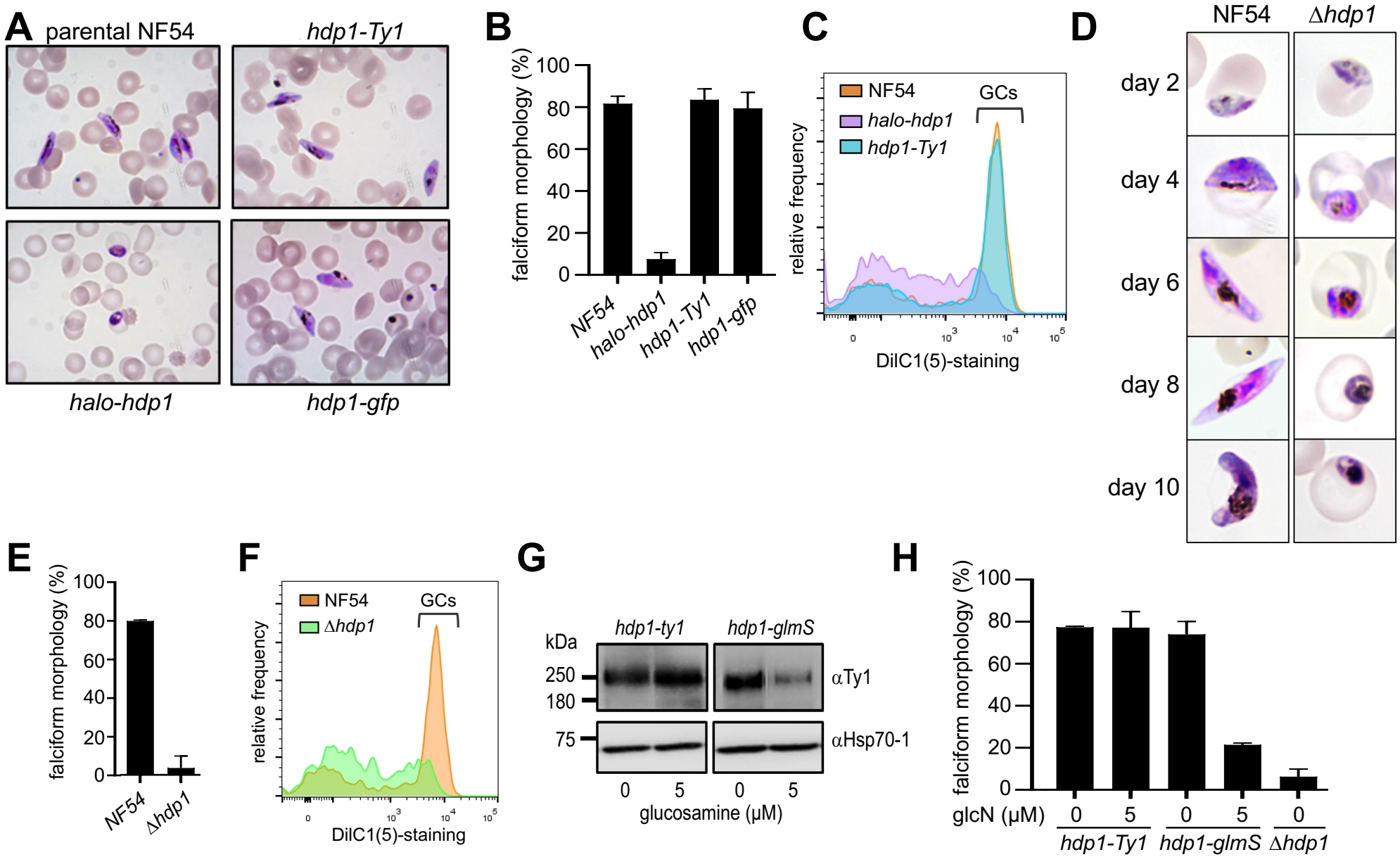

Figure 2: Loss of PfHDP1 function disrupts gametocyte maturation. (A-C) N-terminal tagging of the endogenously encoded HDP1 (*halo-hdp1*) blocked maturation of gametocytes (GCs) while C-terminal tagging of the endogenous locus with either GFP (*hdp1-gfp*) or a triple Ty1 (*hdp1-ty1x3*) epitope had no effect on gametocyte morphology or viability, as determined by membrane potential staining with DilC(1)-5 on day 5 of gametocyte maturation. **(D-F)** Targeted disruption of the *hdp1* locus (Δ*hdp1*) similarly blocked gametocyte maturation. Bar graphs show mean±s.e.m of n=3 **(G)** Glucosamine-inducible knockdown of HDP1 in *hdp1-Ty1* and *hdp1-glmS* day 5 gametocytes. Representative of n=3. **(H)** Percentage of falciform day 5 gametocytes in response to 5 mM glucosamine (GlcN). Images and flow cytometry plots are are representative of n=3.

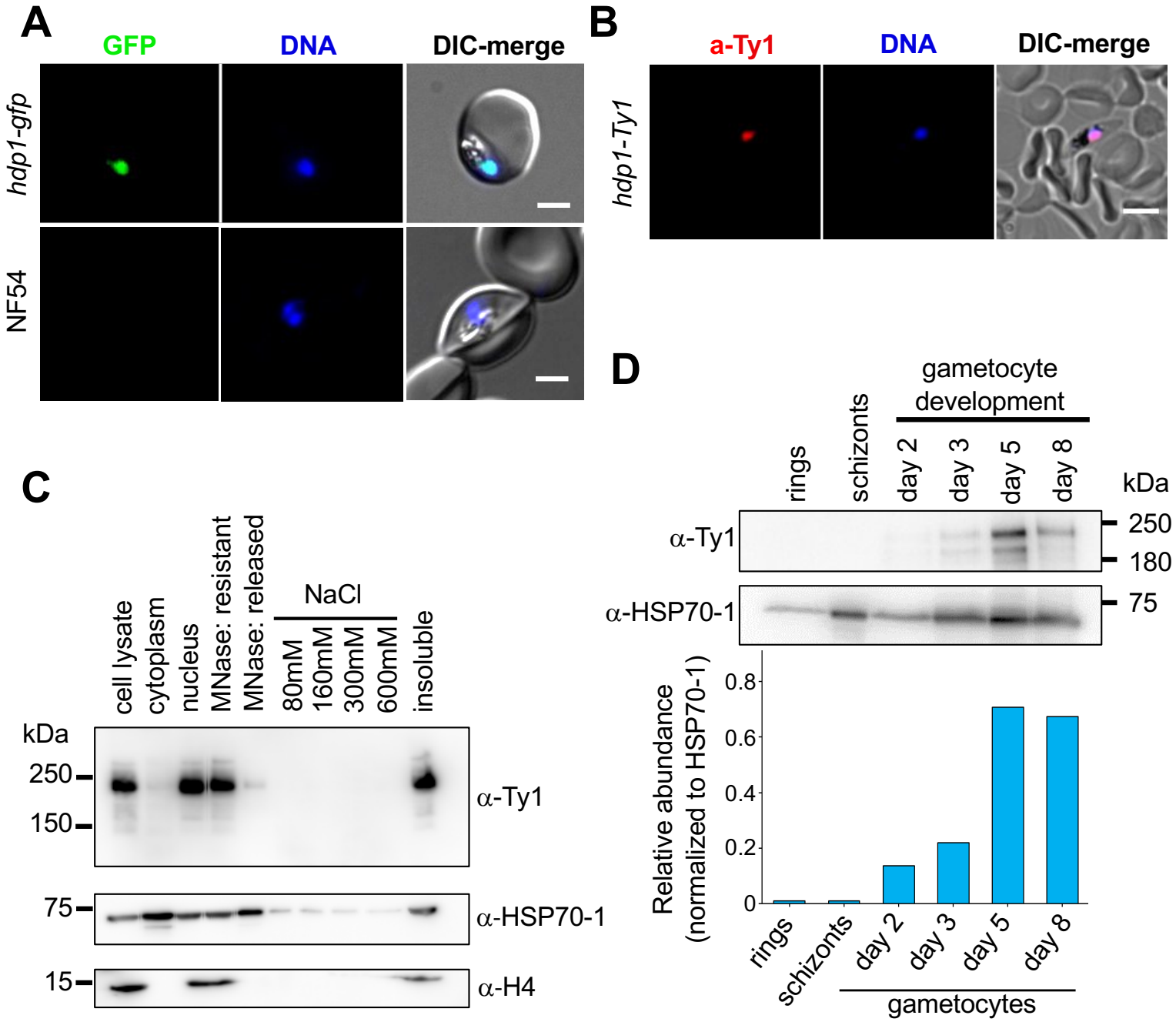

Figure 3: PfHDP1 localizes to the nucleus of gametocytes. (A) Live-cell fluorescence microscopy of *hdp1-gfp* and parental NF54 gametocytes on day 5 of maturation stained with the DNA dye Hoechst33342 (blue). Scale Bar: 2μm. Representative of n=2. **(B)** Immunofluorescence microscopy of hdp1-ty1x3 and parental NF54 gametocytes on day 5 of maturation co-stained with anti-ty1 antibodies (red) and Hoechst33342 (blue). Scale Bar: 5μm. Representative of n=2. **(C)** Western blot of cytoplasmic and nuclear extracts of hdp1-ty1x3 gametocytes on day 5 of maturation with stained with antibodies against the ty1 epitope tag, the histone H4, and HSP70-1. Representative of n=3. **(D)** Western blotting of parasite lysates in asexual stages and during gametocyte maturation shows HDP1 is expressed during the stages of gametocytogenesis. Representative of n=3.

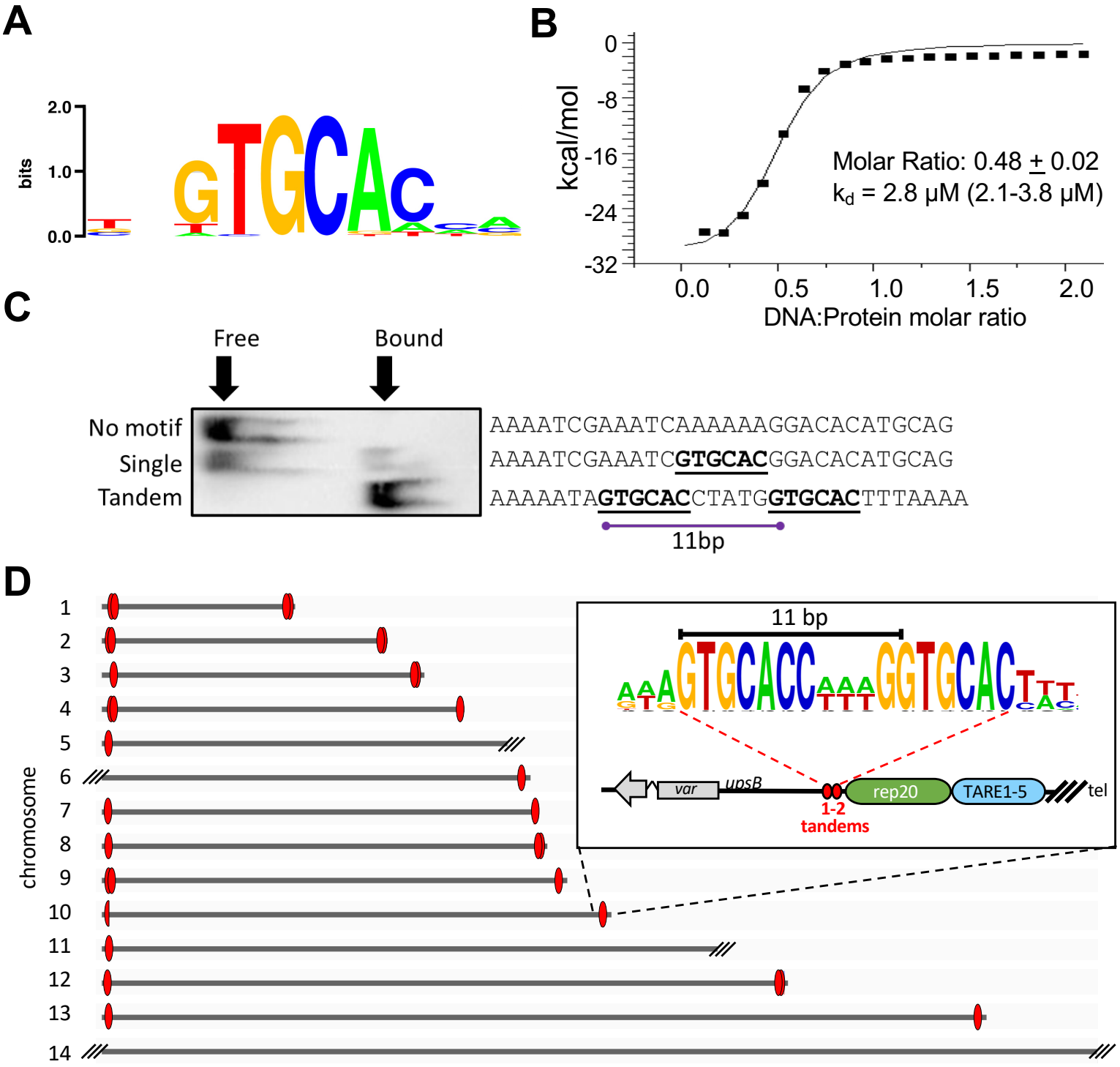

Figure 4: The HDP1 HTH domain dimers recognize a tandem GC-rich motif found at chromosome ends. (A) Maximum enrichment DNA motif for for the GST-HDP1 HTH domain from a protein-binding microarray. **(B)** Isothermal calorimetry indicates the HDP1-HTH domain recognizes DNA as a dimer. n=2. **(C)** Optimal gel-shift was observed for probes containing a tandem motif with a 5bp spacer compared to probes with either a single or no motif. Representative of n=3. **(D)** Tandem HDP1 motifs with a 5-6bp spacer occur exclusively in arrays of 1-2 copies within either 7 bp or 28 bp of the last *rep20* sub-telomeric repeats at all full-length chromosome ends. The motif on the left end of chromosome 10 is degenerate but its positioning is conserved. Truncation by telomere healing resulted in the loss of rep20 adjacent region at five other chromosome ends.

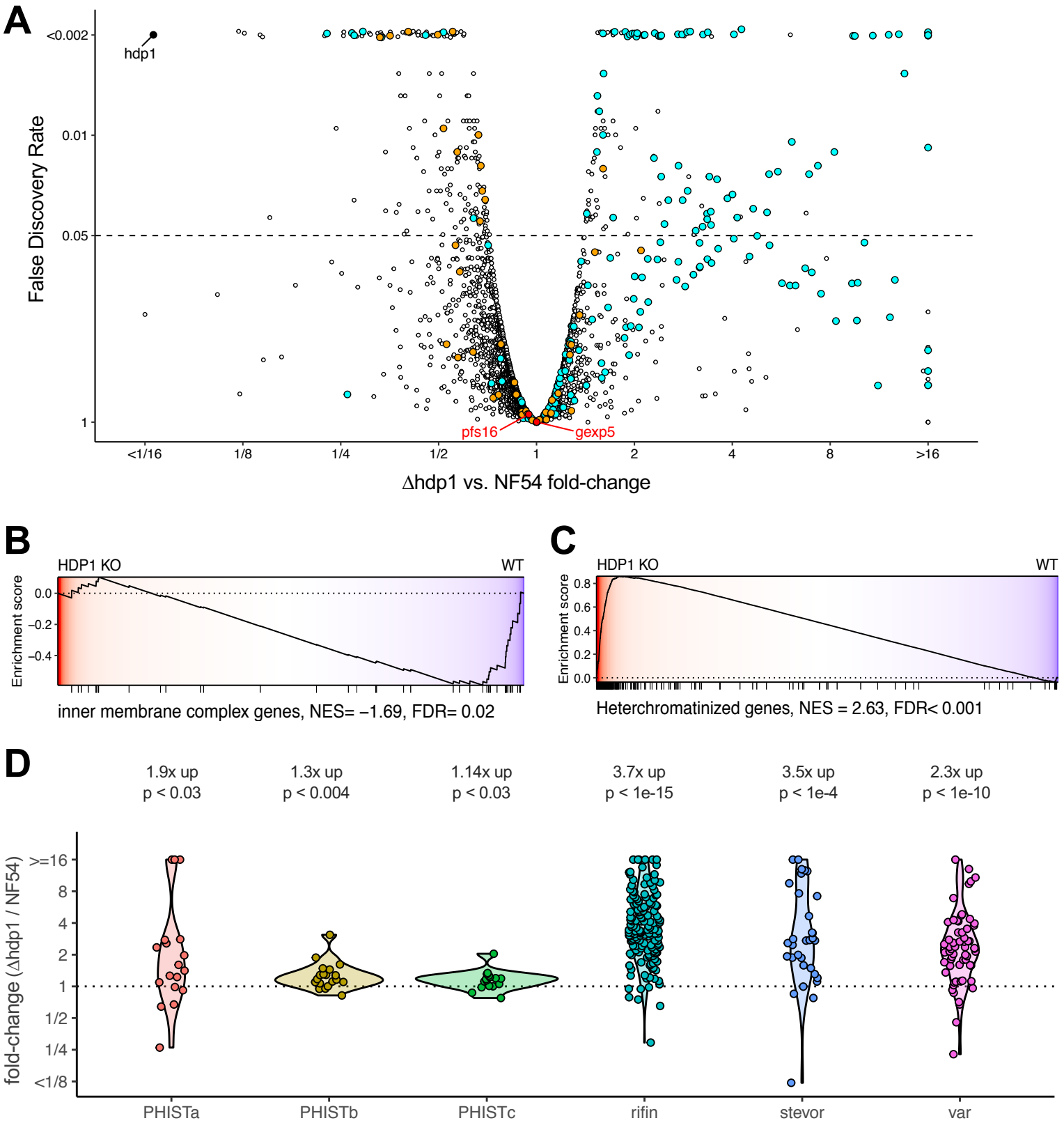

Figure 5: Disruption of HDP1 results in leaky expression of heterochromatin-associated genes and reduced expression of inner membrane complex genes in early gametocytes. **(A)** Genome-wide comparison of differential gene expression in Δ*hdp1* and parental NF54 gametocytes on day 2 of gametocytogenesis (stage I, n=2). *hdp1* (solid black), heterochromatin-associated genes (cyan), IMC genes (orange) and the two canonical early gametocyte markers, *pfs16* and *gexp5 (red)* are highlighted. Gene set enrichment analysis (GSEA) indicated significant downregulation of IMC genes **(B)** and global upregulation of heterochromatin associated genes **(C)**. **(D)** Heterochromatin associated gene families with significant up regulation in Δhdp1. Geometric mean fold-changes and p-values (two-sided, one sample t-test) are indicated.

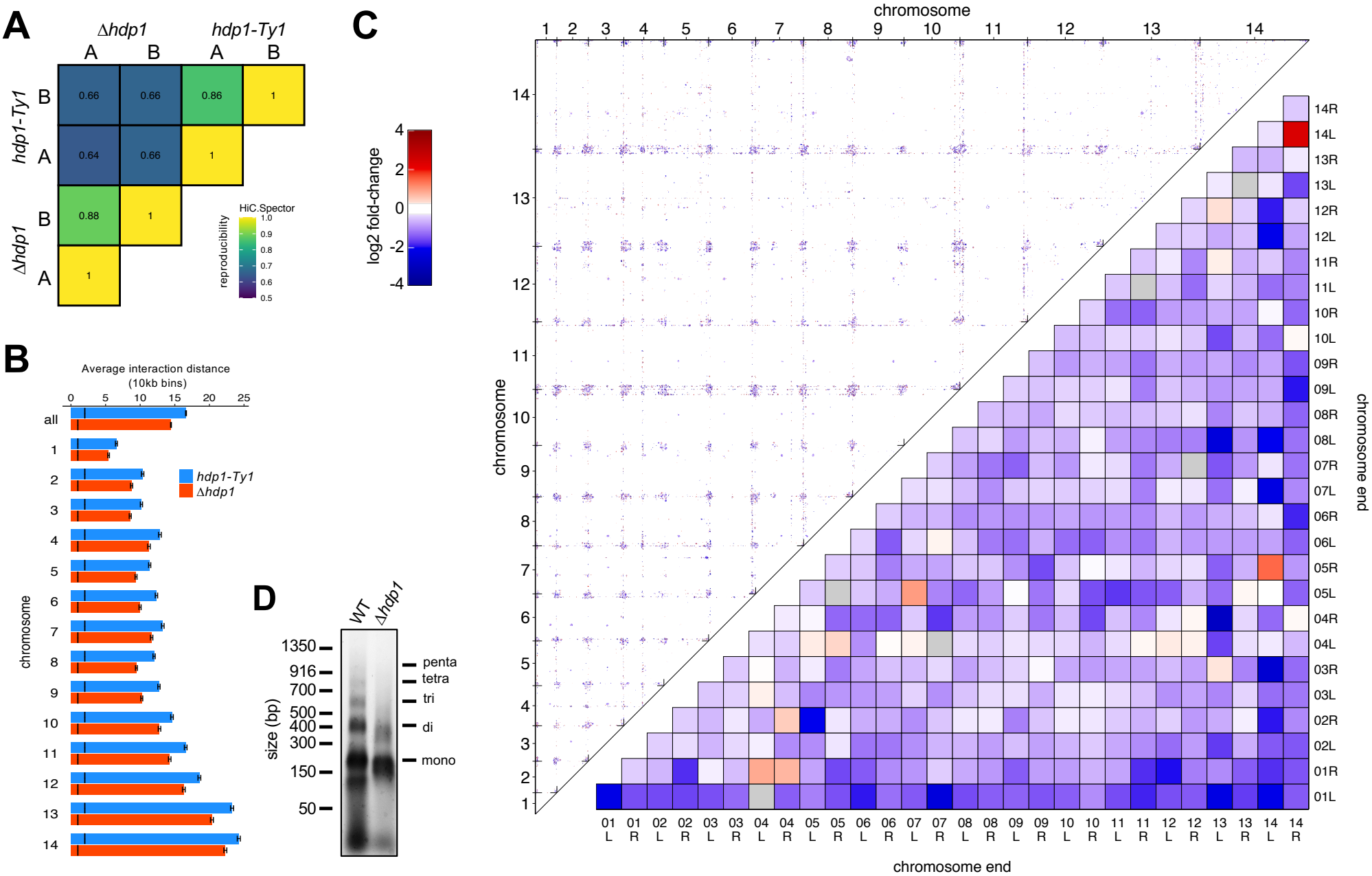

Figure 6: Loss of HDP1 results in reduced telomere clustering. (A) Analysis of Hi-C interaction maps for each sample by HiCSpector highlights reproducibility of replicates and illustrate systematic differences between the strains. Scale ranges from 0-1.0 but only 0.6-1.0 is shown for improved visibility. **(B)** Mean HiC interaction distance in *hdp1-ty1* (blue) and Δ*hdp1* (red) stage I gametocytes. Error-bars indicate the 95% confidence interval and the black line indicates the median interaction distance. **(C)** Top triangle shows significant genome-wide changes in the Δhdp1 compared to hdp1-ty1 with inside ticks indicating chromosome boundaries. FDR < 0.1. The average interaction fold-changes for all pair-wise interactions of chromosome ends are shown in the bottom triangle. **(D)** Accelerated MNase digestion of Δ*hdp1* chromatin from stage I gametocytes indicates reduced chromatin compaction.

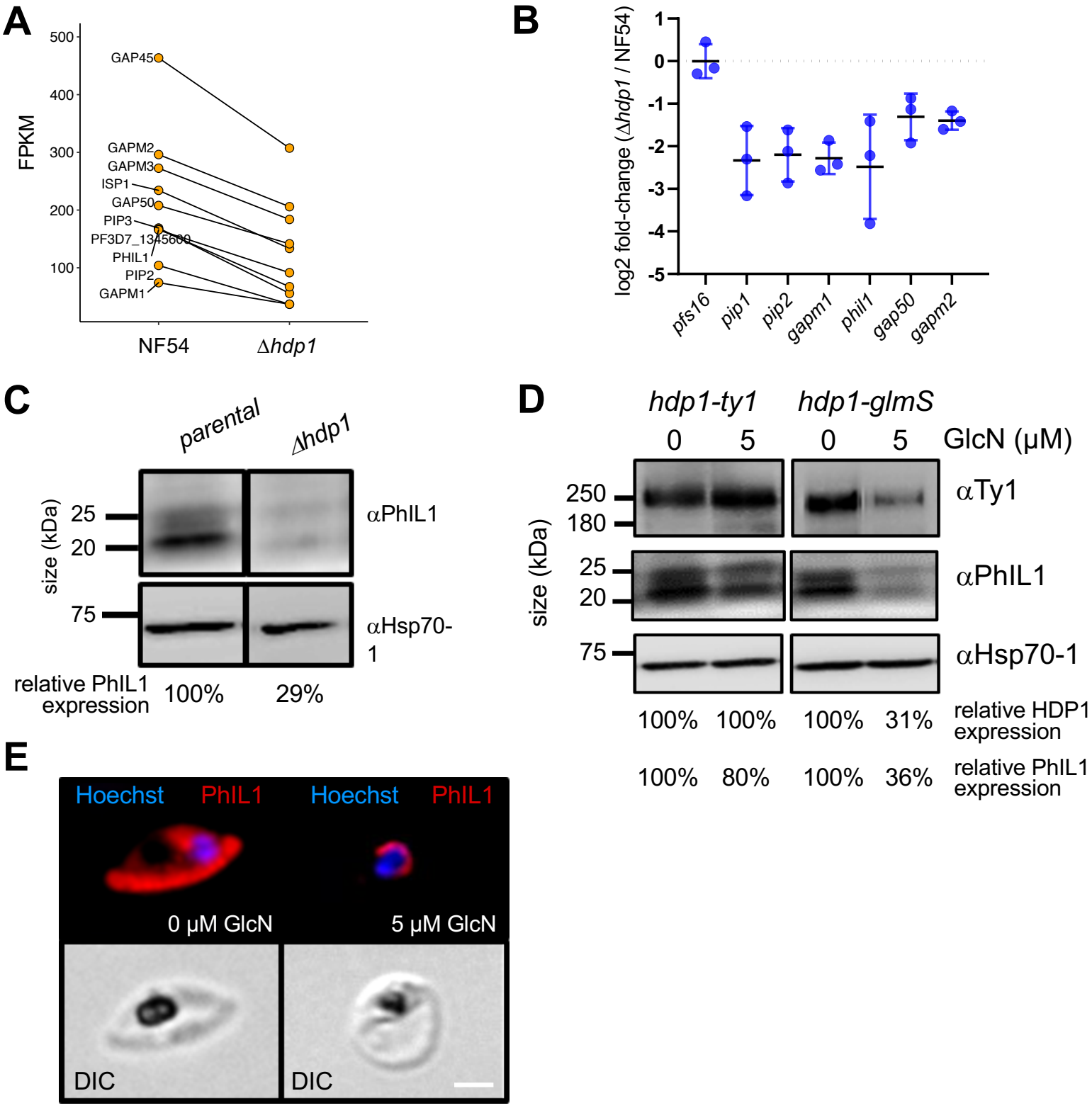

Figure 7: HDP1 regulates PhIL1-dependent expansion of the inner membrane complex in early gametocytes. (A) Transcripts encoding inner membrane complex proteins are down-regulated in Δ*hdp1* day 2 gametocytes. Normalized transcript levels (FPKM) in NF54 and Δ*hdp1* day 2 gametocytes. **(B)** Validation of down-regulation by qRT-PCR. Levels of the canonical early gametocyte marker *pfs16* remained unchanged. (n=3) **(C)** PhiL1 protein levels in parental and Δ*hdp1* day 5 gametocytes. Hsp70-1 abundance shown as the loading control. Representative result of n=2. **(D)** Day 5 morphology of *hdp1-ty1* and *hdp1-glmS* gametocytes under 0 and 5 μM glucosamine. HDP1 and PhiL1 protein levels in *hdp1-ty1* and Δ*hdp1* day 5 gametocytes. Hsp70-1 abundance shown as the loading control. Representative result of n=3. **(E)** Immunofluorescence microscopy of PhiL1 distribution in day 5 gametocytes of *hdp1-glmS* under 0 and 5 μM glucosamine. Scale Bar: 3μm

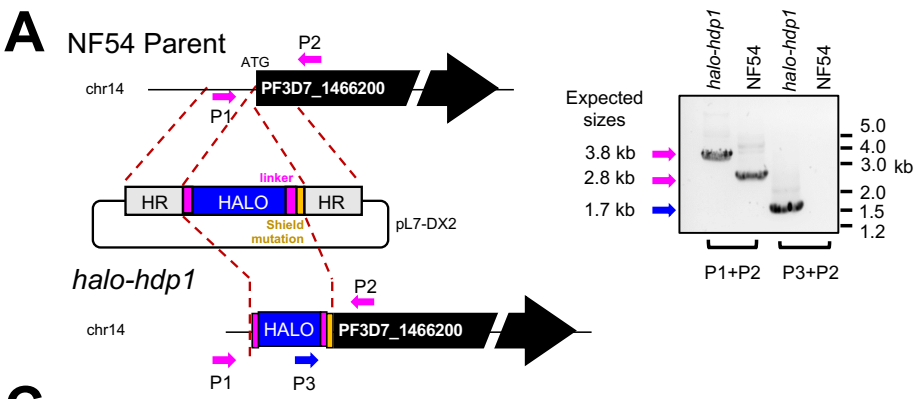

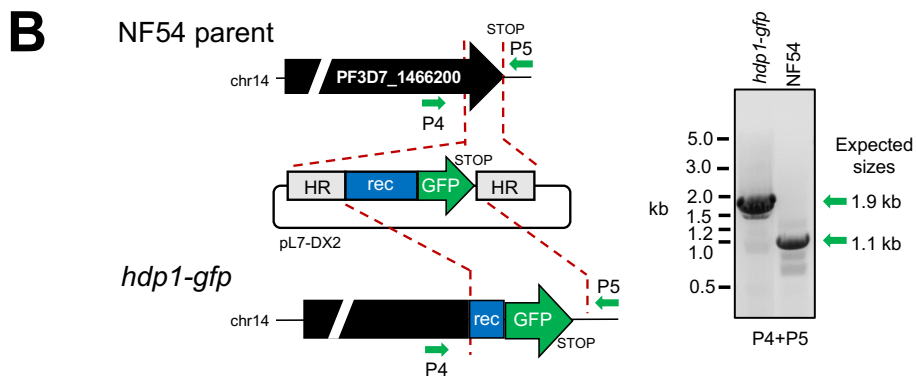

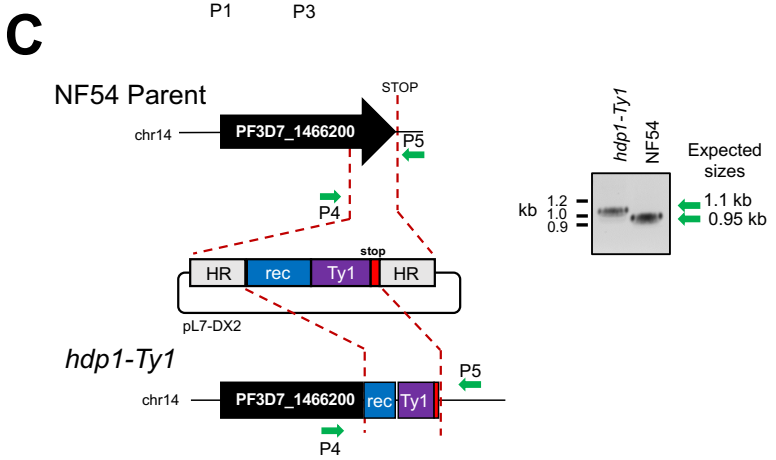

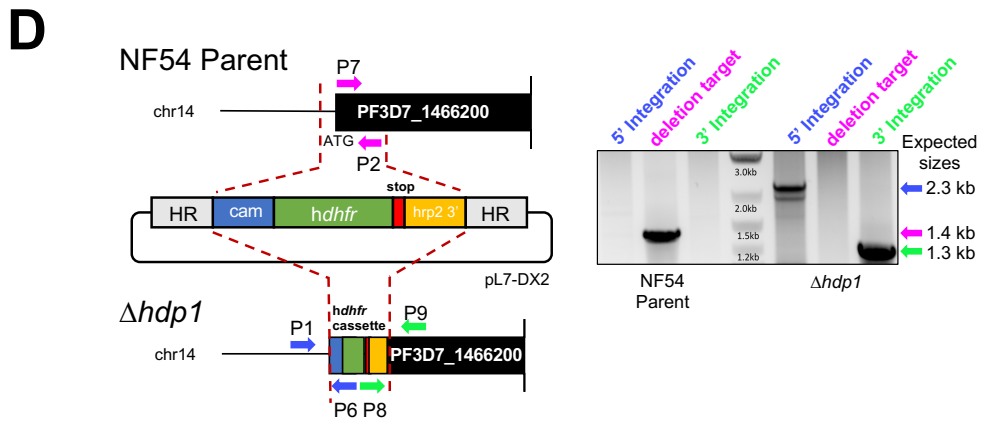

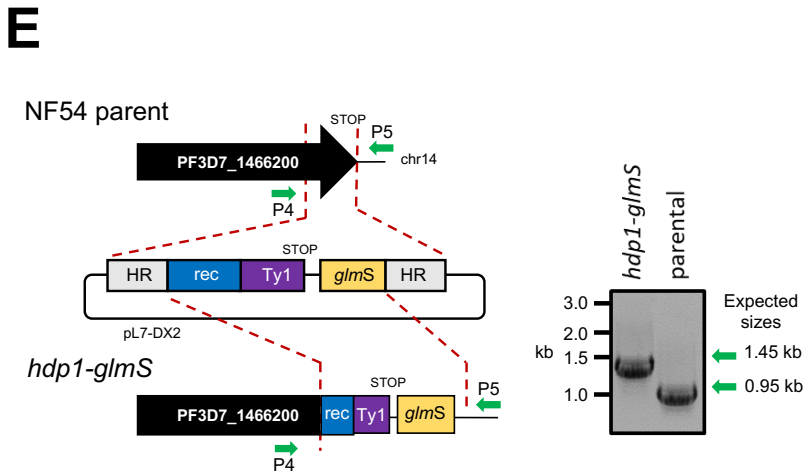

Figure S1: Validation of engineered parasite lines. (A) Generation of h*alo-hdp1* parasites by CAS9 genome editing. Insertion of the N-terminal HALO tag at the 5' end the *hdp1* coding sequence was confirmed by PCR and checked for mutations by Sanger sequencing of the 3.8kb PCR product (not shown). **(B)** Generation of *hdp1-gfp* parasites by CAS9 genome editing. Insertion of the C-terminal GFP tag at the 3' end the *hdp1* coding sequence was confirmed by PCR and checked for mutations by Sanger sequencing of the 1.9kb PCR product (not shown). **(C)** Generation of *hdp1-Ty1* parasites by CAS9 genome editing. Insertion of the C-terminal triple Ty1 epitope tag at the 3' end the *hdp1* coding sequence was confirmed by PCR and checked for mutations by Sanger sequencing of the 1.1kb PCR product (not shown). **(D)** Generation of Δ*hdp1* parasites by CAS9 genome editing. Replacement of 1.4 kb flanking the *hdp1* start codon by a hDHFR selectable marker cassette was confirmed by PCR. **(E)** Generation of *hdp1-glmS* parasites by CAS9 genome editing. Insertion of the C-terminal triple Ty1 epitope tag and the glmS ribozyme at the 3' end the *hdp1* coding sequence was confirmed by PCR and checked for mutations by Sanger sequencing of the 1.4 kb PCR product (not shown).

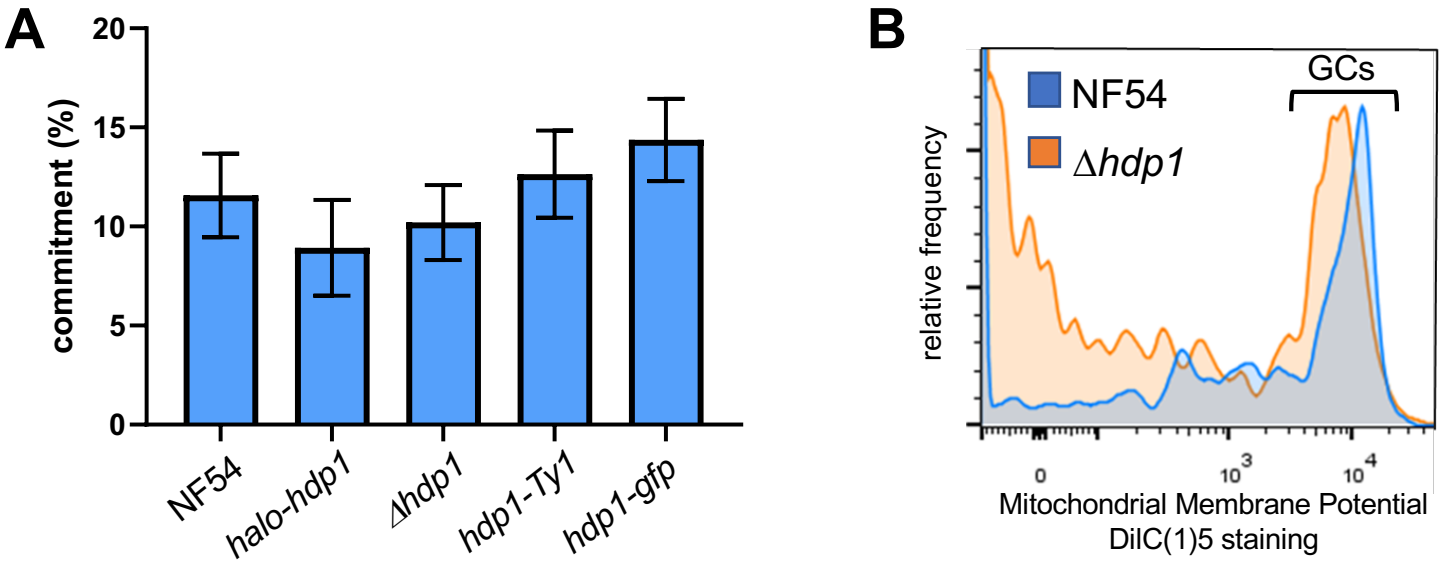

Figure S2: Loss of HDP1 does not alter the sexual commitment frequency or Stage I gametocyte viability. (A) The sexual commitment frequency (day 5 gametocytes per day 1 ring stages) is not significantly affected in *halo-hdp1* and Δ*hdp1* parasites. n=3 **(B)** Mitochondrial membrane potential as measured by DilC(1)5 staining indicates similar viability of day 2 gametocytes (GCs) from NF54 (blue) and Δ*hdp1* (orange). Representative of n=2.

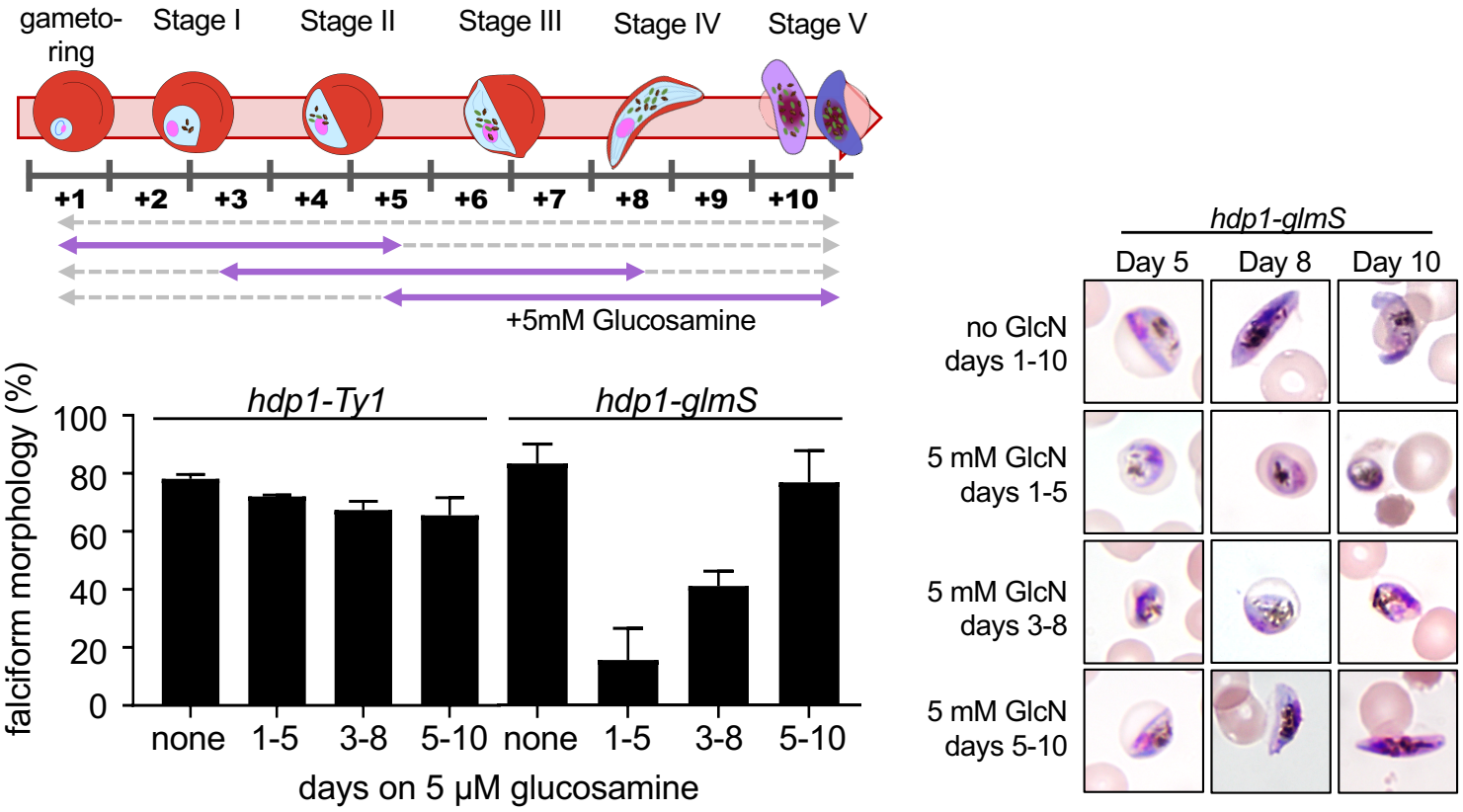

Figure S3: Inducible knockdown of HDP1 reduces gametocyte maturation in early but not late gametocytes. Representative morphology (right) of hdp1-glmS gametocytes in response to 5mM glucosamine on days 1-10, 3-8, 5-10, or in the absence of glucosamine. Percentage of falciform gametocytes on Day 10 in response to 5 mM glucosamine on days 1-10, 3-8, 5-10, or in the absence of glucosamine for hdp1-Ty1 or hdp1-glmS parasites (bottom). mean±s.e.m of n=3.

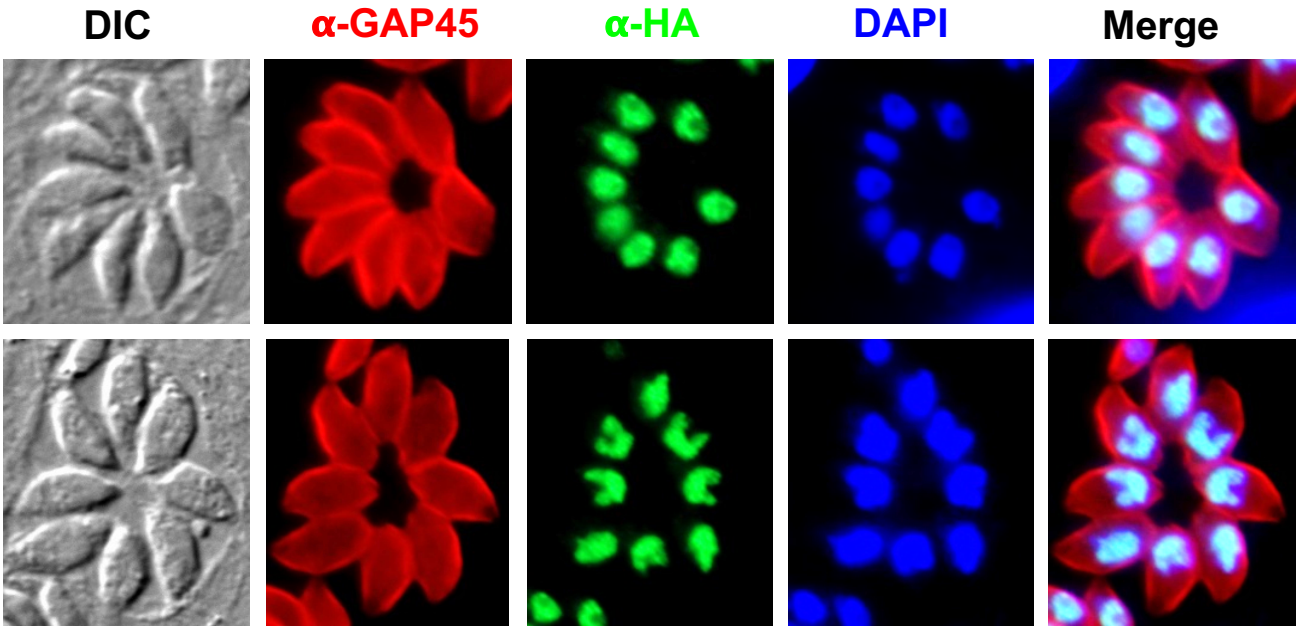

Figure S4: Immunofluorescence microscopy localizes the HA-tagged ortholog TGME49_233160 to the nucleus of *Toxoplasma gondii* tachyzoites.

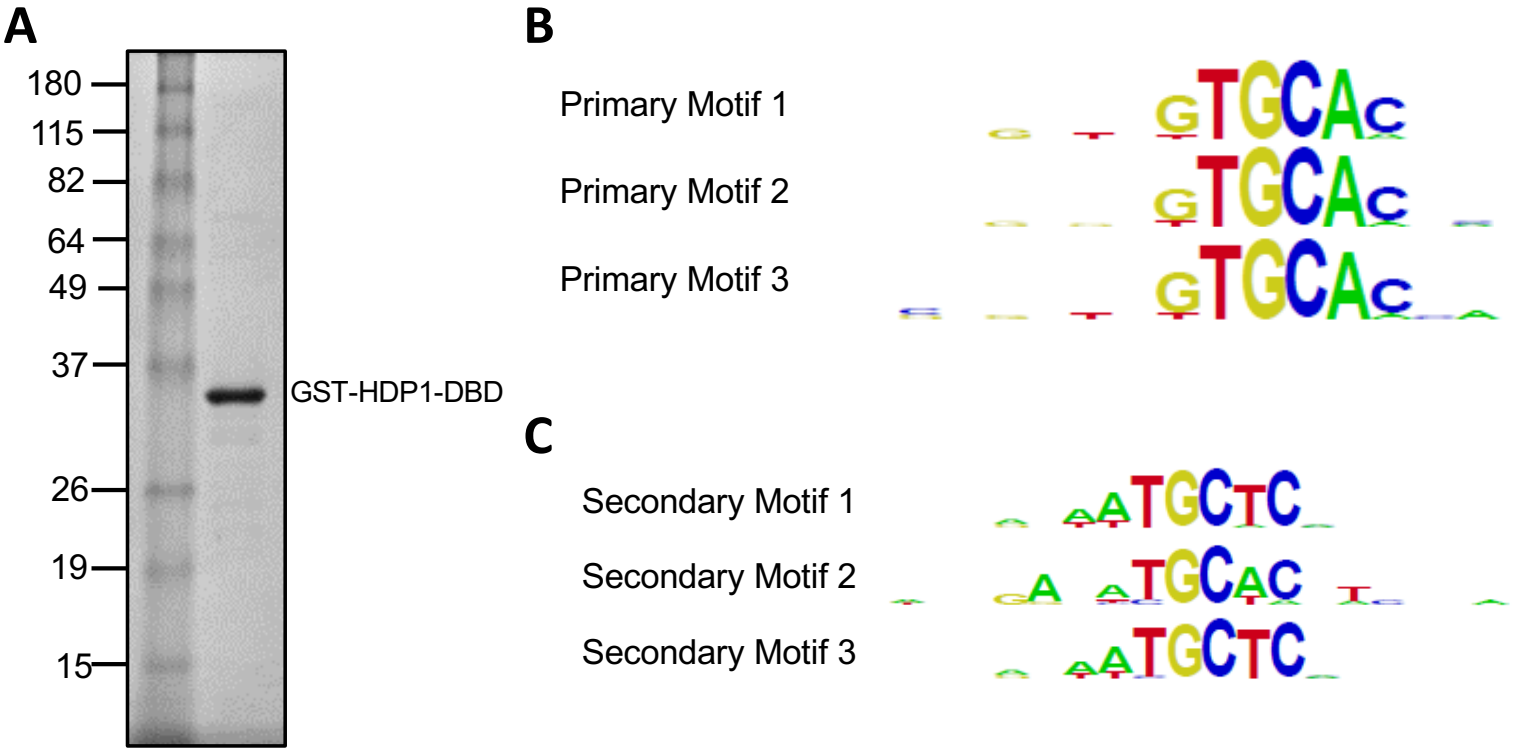

Figure S5: HDP1 binds to a GC-rich motif on Protein Binding Microarray (A) Coomassie stain of GST-HDP1-DBD used for PBM analysis. **(B)** Top three primary motif hits. **(C)** Top three secondary motif hits after removal of primary hits.

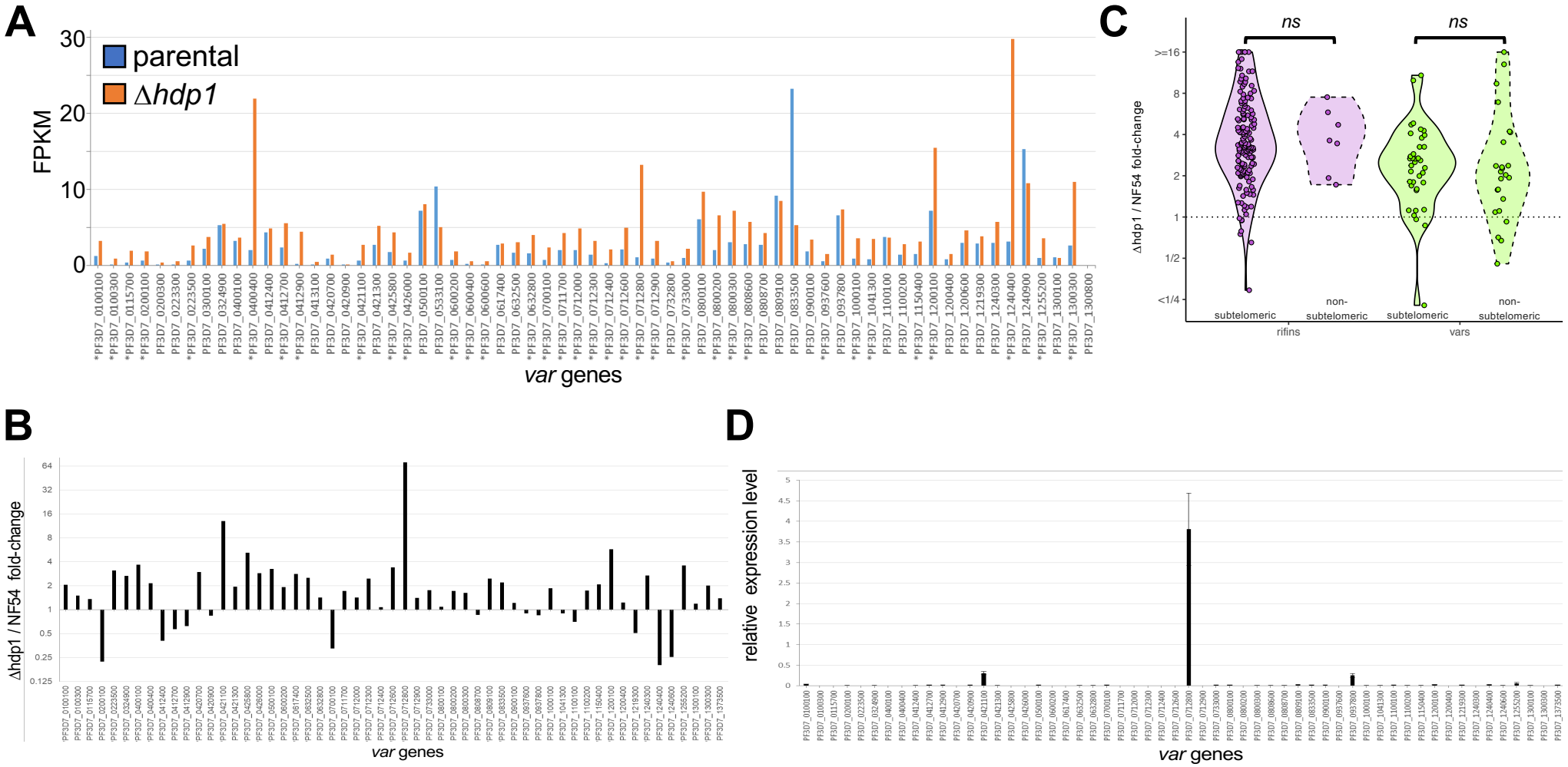

Figure S6: *var* gene expression is altered in early Δ*hdp1* gametocytes but not asexual blood stages. (A) Normalized abundance of reads uniquely mapping to *var* genes in day 2 gametocytes from Δ*hdp1* (orange) or parental NF54 parasites (blue). Significantly upregulated genes are marked with asterisks. (n=2) **(B)** qRT-PCR confirmation of *var* gene up-regulation in Δ*hdp1* vs NF54 day 2 gametocytes. **(C)** Upregulation of *rifin* (purple) and *var* genes (green) in Δ*hdp1* day 2 gametocytes is independent of chromosomal position in subtelomeric or non-subtelomeric heterochromatin clusters. **(D)** qRT-PCR analysis of *var* transcript abundance (normalized seryl tRNA synthetase expression) in Δ*hdp1* asexual ring stages found expression a single dominant var as expected indicating that mutually exclusive expression remains unchanged in asexual stages. (n=2)

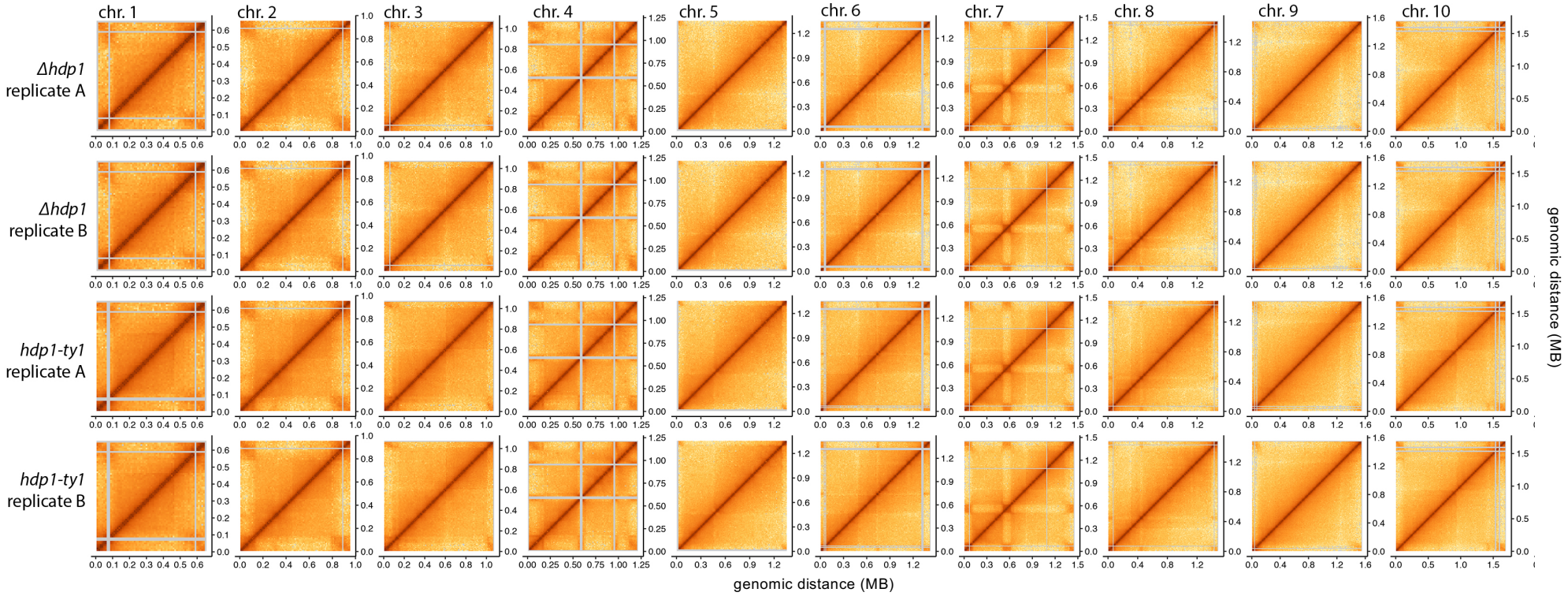

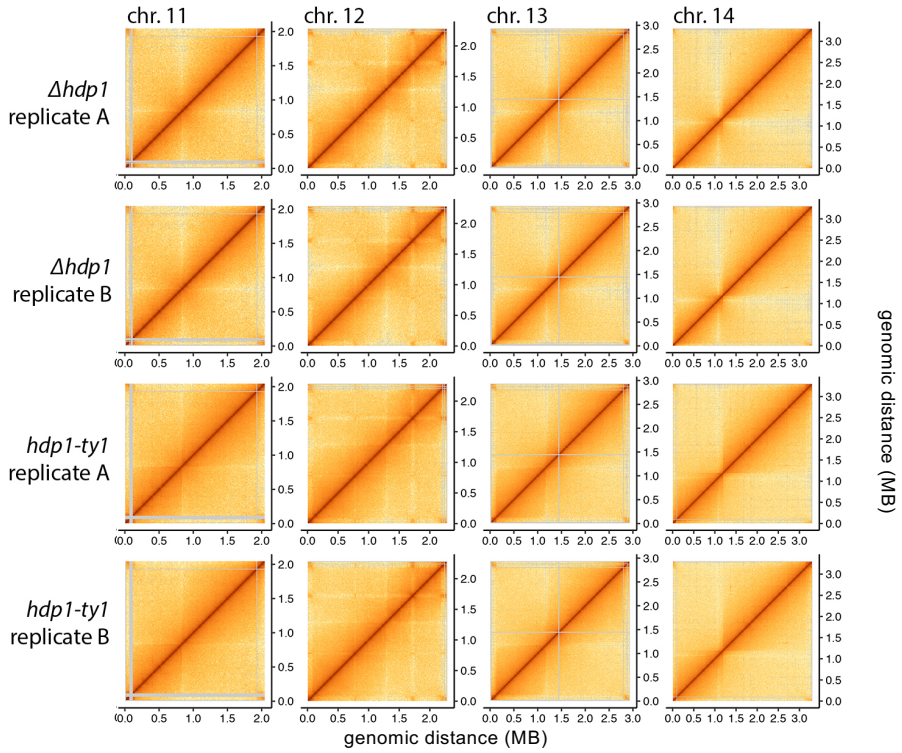

Figure S7 Intra-chromosomal HiC maps from Δ*hdp1* (top) and *hdp1-Ty1* (bottom) of day 2 gametocytes. Color scale indicates the normalized log10 interaction frequency (counts per million). Gray bars indicate bins of high-homology that could not be uniquely mapped with high confidence.